AD-A112 175 AERONAUTICAL RESEARCH LABS MELBOURNE (AUSTRALIA) F/G 20/11
CRACK CLOSURE AND CRACK GROWTH RATE: AN EMPIRICAL MODEL TO ACCO--ETC(U)
AUG 81 G S JOST, L R GRATZER
UNCLASSIFIED ARL/STRUC-387 NL

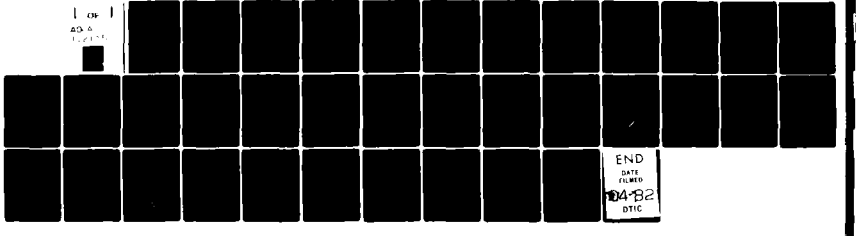

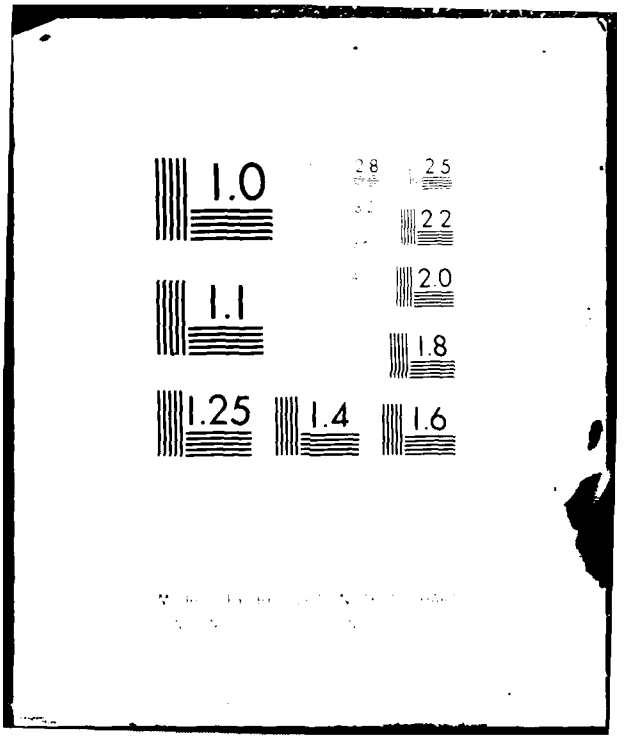
1.0
2.8
2.5
2.2
2.0
1.1
1.8
1.25
1.4
1.6

ARL/STRUC-REPORT-387 AR-002-311

DEPARTMENT OF DEFENCE

DEFENCE SCIENCE AND TECHNOLOGY ORGANISATION

AERONAUTICAL RESEARCH LABORATORIES

MELBOURNE, VICTORIA

STRUCTURES REPORT 387

CRACK CLOSURE AND CRACK GROWTH RATE: AN EMPIRICAL MODEL TO ACCOUNT FOR R

by

G. S. JOST and L. R. GRATZER

Approved for Public Release.

COPY No

82 03 20 095

August 1981

AR-002-311

DEPARTMENT OF DEFENCE
DEFENCE SCIENCE AND TECHNOLOGY ORGANISATION
AERONAUTICAL RESEARCH LABORATORIES

STRUCTURES REPORT 387

CRACK CLOSURE AND CRACK GROWTH RATE: AN EMPIRICAL MODEL TO ACCOUNT FOR R

by

G. S. JOST and L. R. GRATZER

SUMMARY

An empirical equation is proposed to account for stress ratio effects in fatigue crack growth based upon the crack closure concept. It is characterised by two fitted parameters.

The new equation is used to establish effective stress intensity ranges for three sets of extensive crack growth rate data from the literature covering the stress ratio range $-1 \leqslant R < 1$. *Least squares best fitted Paris equations are then used to predict crack growth lives for comparison with the individual originals. Actual lives are almost invariably within the range from 1/3 to 2 times those predicted.*

The study shows that even better fits to the data would result from using a sigmoidal growth rate/effective stress intensity range relationship. This approach is being followed up.

POSTAL ADDRESS: Chief Superintendent, Aeronautical Research Laboratories,
Box 4331, P.O., Melbourne, Victoria, 3001, Australia.

DOCUMENT CONTROL DATA SHEET

Security classification of this page: Unclassified

1. Document Numbers
   (a) AR Number:
   AR 002 311
   (b) Document Series and Number:
   Structures Report 387
   (c) Report Number:
   ARL Struc Report 387

2. Security Classification
   (a) Complete document:
   Unclassified
   (b) Title in isolation:
   Unclassified
   (c) Summary in isolation:
   Unclassified

3 Title: CRACK CLOSURE AND CRACK GROWTH RATE: AN EMPIRICAL MODEL TO ACCOUNT FOR *R*

4. Personal Author(s):
   G. S. Jost
   L. R. Gratzer

5. Document Date:
   August, 1981

6. Type of Report and Period Covered:

7. Corporate Author(s):
   Aeronautical Research Laboratories

8. Reference Numbers
   (a) Task:
   DST 76 156
   (b) Sponsoring Agency:

9. Cost Code:
   27 7030

10. Imprint:
    Aeronautical Research Laboratories, Melbourne

11. Computer Program(s)
    (Title(s) and language(s)):

12. Release Limitations (of the document)
    Approved for Public Release

12.0. Overseas:	N.O.		P.R.	1	A		B		C		D		E	

13. Announcement Limitations (of the information on this page):
    No Limitations

14. Descriptors:
    Crack propagation
    Cracking (fracturing)
    Fatigue (materials)
    Str[illegible]ratio
    Crack closure

15. Cosati Codes:
    1113
    2012

16.

ABSTRACT

An empirical equation is proposed to account for stress ratio effects in fatigue crack growth based upon the crack closure concept. It is characterised by two fitted parameters.

The new equation is used to establish effective stress intensity ranges for three sets of extensive crack growth rate data from the literature covering the stress ratio range $-1 \leq R < 1$. *Least squares best fitted Paris equations are then used to predict crack growth lives for comparison with the individual originals. Actual lives are almost invariably within the range from 1/3 to 2 times those predicted.*

The study shows that even better fits to the data would result from using a sigmoidal growth rate, effective stress intensity range relationship. This approach is being followed up.

CONTENTS

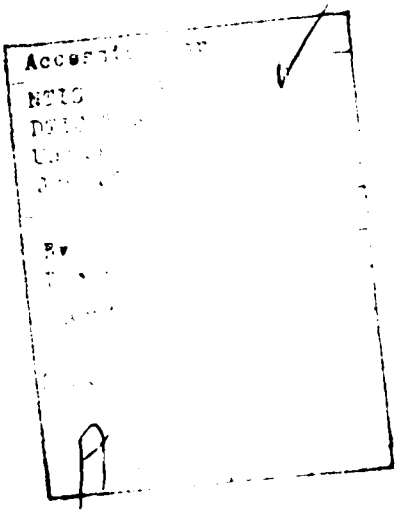

1. INTRODUCTION

The significance of the observation by Elber[1] that the fracture surfaces of cracks in specimens undergoing tensile fatigue loadings remain closed during the lower stress part of the cycle has now become generally appreciated. There can be no doubt that the phenomenon must modify substantially the manner in which the behaviour of cracked regions to subsequent fatigue loading is assessed: in particular, allowance for consideration of crack closure in predictive fatigue crack growth modelling would seem to be mandatory.

In this Report, several empirical models which have been proposed for relating crack closure to stress ratio are considered briefly, and a more flexible empirical model, free of most of the limitations of earlier models, is presented. The ability of the new model to condense crack growth rate data obtained at several stress ratios is then examined. Finally, predicted crack growth curves obtained from the condensed growth rate data are compared with experimental data, and reveal (surprisingly) little scatter.

2. MODELS FROM THE LITERATURE

In this Section several models from the literature relating crack closure under constant amplitude loading and stress ratio are examined and compared.

2.1 Elber, 1971[1]

The first proposal relating crack opening stress*, S_{op}, and the other cycle stresses S_{max} and S_{min} to stress ratio R was made by Elber in the form

$$U = (S_{max} - S_{op})/(S_{max} - S_{min}) = f(R) \tag{1}$$

where U was defined as the effective stress range ratio. For 2024-T3 aluminium alloy data he found that

$$U = 0{\cdot}4R + 0{\cdot}5 \tag{2}$$

approximately, in the range $-0{\cdot}1 \leq R \leq 0{\cdot}7$.
From (1) and (2)

$$S_{op}/S_{max} = 0{\cdot}4R^2 + 0{\cdot}1R + 0{\cdot}5. \tag{3}$$

This expression is shown as the upper curve in Fig. 1, along with the data on which it is based. Schijve[2] has pointed out that since (3) has a minimum at $R = -0{\cdot}125$ it cannot physically be correct for $R < -0{\cdot}125$ where the crack opening stress must continue either to decrease or be asymptotic to some constant low level.

2.2 Bell and Creager, 1974[3]
Bell and Wolfman, 1976[4]
Eidinoff and Bell, 1977[5]

In modelling crack growth under variable amplitude sequences, the above authors have also used the concepts of crack closure. They have fitted empirical equations of the following form

* No distinction is made here between opening stress and closing stress. Although the phenomenon is known as crack closure, it is actually crack opening during the increasing part of the loading cycle which is of interest.

to aluminium and titanium alloy data in the range $-1 < R < 1$.

$$S_{op}/S_{max} = (S_{op}/S_{max})_1 + [(S_{op}/S_{max})_0 - (S_{op}/S_{max})_1](1 - R)^p \quad (4)$$

where the subscripts 1 and 0 refer to R values. This equation has flexibility in that the opening stress ratio S_{op}/S_{max} must be specified at $R = 0$ and $R = 1$, along with the exponent p. On the other hand, there is a major deficiency: at $R = 1$ the value of S_{op}/S_{max} does not necessarily equal one as is required: as $R \to 1$, the minimum stress approaches the maximum as must the opening stress. Representative values of the constants from Reference 5 for four aluminium alloys and three titanium alloys are given in Table 1, their plots being shown in Figure 2. Figure 3 shows a redrawing of Figure 2B of Reference 5, highlighting the variability which is a feature of crack opening measurements.

2.3 Newman, 1976[6]

Newman carried out a two-dimensional finite element analysis using an elastic-perfectly plastic material to predict crack closure and crack opening stresses during cyclic loading. Predictions were made at R values of $-1{\cdot}0$, $-0{\cdot}5$, 0 and $0{\cdot}5$ using two values of the ratio of maximum stress to yield stress. When $R \geq 0$, and irrespective of the S_{max}/S_{yield} values used, predictions agreed very closely with those of Elber, Figure 1. However, for $R < 0$ differences in predicted S_{op}/S_{max} appear, according to the ratio S_{max}/S_{yield}: the larger this latter, the lower is S_{op}/S_{max}. More importantly for present purposes, however, the predictions confirm the intuitive notion of an (asymptotic?) decrease in S_{op}/S_{max} for increasingly negative R.

2.4 Schijve, 1979[7]

Schijve has adopted a cubic polynomial and used it to condense 2024-T3 Alclad crack growth rate data in the range $-1 \leq R \leq 1$:

$$S_{op}/S_{max} = 0{\cdot}1R^3 + 0{\cdot}25R^2 + 0{\cdot}2R + 0{\cdot}45 \quad (5)$$

This equation is very similar to that of Elber for $R > 0$, but corrects its unsatisfactory performance for $R < 0$, Figure 1. Schijve points out that (5) has a very weak minimum at $R = -0{\cdot}67$: it also has a weak maximum at $R = 1$. Both slope $(S_{op}/S_{max})'$ and magnitude S_{op}/S_{max} are unity at $R = 1$.

Although no explanation is offered as to how the coefficients in (5) were determined, it will be seen later that the collective choice is a very happy one for the particular data used. Differing data may well require other coefficient values – their determination will be no simple task if a satisfactory solution is to be found by trial and error.*

2.5 Summary

1. Schijve's formulation for 2024-T3 in the range $-1 \leq R \leq 1$ represents a significant improvement over that of Elber, which was limited to the range $-0{\cdot}1 \leq R \leq 0{\cdot}7$.

2. Newman's finite element predictions confirm the general trend of a flattening out of the S_{op}/S_{max} versus R curve for increasingly negative R. For $R > 0$, the predictions agree well with those of Elber and Schijve.

3. The model of Bell and co-authors, for the range $-1 \leq R \leq 1$, although possessing unusual limiting values for some materials, does have a flexibility which the other analytical models lack. Although values are required for three constants in each formulation, the curves of Figure 2, for two alloy groups, suggest that a family of curves formed from some basic curve might suffice. This idea is pursued in the following.

* Since this Report was written, further Dutch activity in this area has been published (Refs. 12 and 13).

3. PROPOSAL

The crack opening data and the forms of the empirical models reviewed in Section 2 and shown in Figures 1 and 2, suggest the following boundary conditions, which have been adopted here, for the relationship between S_{op}/S_{max} and R:

1. S_{op}/S_{max} 1 at R 1
2. $(S_{op}/S_{max})'$ 1 at R 1
3. $(S_{op}/S_{max})'$ 0 at some specified low value of R, X say, below which S_{op}/S_{max} is constant.
4. $(S_{op}/S_{max})'' > 0$ in the range $X \leq R \leq 1$,

   i.e. there are no points of inflexion. By setting $(S_{op}/S_{max})''$ 0 at R X, the second derivative (as well as the first) becomes continues into the (constant S_{op}/S_{max}) region beyond R X.

A cubic polynomial in R conforming to the above boundary conditions has, for given X, the following unique solution:

$$(S_{op}/S_{max})_{int} \quad \frac{R^3 \quad 3XR^2 \quad 3X^2R \quad (3X \quad 2)}{3(X \quad 1)^2} \tag{6}$$

where the subscript refers to an intermediate stage in the process of establishing a relationship between S_{op}/S_{max} and R.

For X 1, the lower limit of R considered by most of the models examined in Section 2, (6) becomes

$$(S_{op}/S_{max})_{int} \quad \frac{R^3}{12} \quad \frac{R^2}{4} \quad \frac{R}{4} \quad \frac{5}{12} \tag{7}$$

This is shown in Figure 4 along with the relationships, eq. 6, for neighbouring values of X.

Although (6) has flexibility in that X may be arbitrarily chosen, the choice automatically fixes the entire curve, including the level of $(S_{op}/S_{max})_{int}$ at R X. According to material, Figures 1 and 2 suggest, for example, a range from about 0·3 to 0·5 at R 1. Clearly, for given X, a shift in S_{op}/S_{max} is required to accommodate this variation, and a suitable one takes the following form:

$$S_{op}/S_{max} \quad (S_{op}/S_{max})_{int}(1 \quad Z(1 \quad S_{op}/S_{max})^2_{int}) \tag{8}$$

where $(S_{op}/S_{max})_{int}$ is a function only of R and X, given here by eq. (6), and Z is a shift parameter. Equation (8) also satisfies the boundary conditions given above. Representative families of shifted S_{op}/S_{max} *versus* R for X 1 and 0·5 are shown in Figure 5.

Thus in the proposed formulation (6) and its shifted version (8) there is complete freedom to choose:

(a) the limiting lower value of R (R X) at which the S_{op}/S_{max} versus R curve reaches zero slope and curvature, and

(b) the required magnitude of S_{op}/S_{max} at this point, by choice of an appropriate value of shift parameter, Z.

Specification of these two parameters defines completely the relationship between S_{op}/S_{max} and R.

4. APPLICATION TO CRACK GROWTH RATE DATA

Elber proposed that crack closure concepts might be useful in explaining the known qualitative effect of stress ratio on crack growth. In particular he suggested that crack growth rate was not so much a function of the stress intensity range ΔK as of the *effective* stress intensity range ΔK_{eff}, i.e. the difference between the maximum stress intensity and that corresponding to crack opening. Thus, in place of ΔK in the Paris equation:

$$da/dN \quad B\Delta K^m$$

where

$$\Delta K \quad K_{max} \quad K_{min},$$

there should be substituted ΔK_{eff}:

$$da\,dN \quad C\Delta K_{eff}^{n} \tag{9}$$

where

$$\Delta K_{eff} \quad K_{max} \quad K_{op}.$$

Since the crack opening stress, S_{op}, is a function of R (eqs 6 and 8) the crack opening stress intensity K_{op} is also a function of R. Thus, a plot of log $da\,dN$ versus ΔK_{eff}, which includes data at differing R values, should have associated with it only the variability in crack growth rate itself, as was first demonstrated by Elber[1] using data from Reference 8.

The effectiveness of the formulations proposed in Section 3 has been evaluated using three published sets of extensive crack growth data: those of Schijve[7] on 2024-T3 Alclad sheet and those of Hudson[8] on 2024-T3 and 7075-T6 aluminium alloy sheet. These data sets are shown in Figures 6(a), (b) and (c) in terms of the conventional $da\,dN$ versus ΔK plots. The observable groupings of data are associated with the differing R values used on test. Shijve's data on 2024-T3 Alclad sheet are given in the Appendix to Reference 7 in terms of $da\,dN$ and ΔK, and have been so used here; Hudson's data are given in Reference 8 in terms of cycles to given crack lengths. These latter have been fitted by cubic splines, from which the derivatives at the given crack lengths have provided the required $da\,dN$ data*. The corresponding stress intensities were obtained as indicated below.

For the centrally through-cracked specimens used in all three investigations the stress intensity, K, at the crack tip is given by

$$K \quad S\sqrt{(\pi a)}\,F \tag{10}$$

where S is the remote applied stress, a is the semi-crack length and F is the finite width correction factor given by

$$F \quad \sqrt{(\sec \pi a / W)}, \tag{11}$$

W being the total width of the specimen.

The effective stress intensity, ΔK_{eff}, for use in eq. (9) is therefore given by

$$\begin{aligned} \Delta K_{eff} \quad & K_{max} \quad K_{op} \\ & (S_{max} \quad S_{op})\sqrt{(\pi a)}\,F \\ & S_{max}(1 \quad S_{op}/S_{max})\sqrt{(\pi a)}\,F \end{aligned} \tag{12}$$

where S_{op}/S_{max} is the function of R, λ and γ given by equations (6) and (8).

Since ΔK_{eff}, for each R was not measured on test, but is being modelled here by equations (6), (8) and (12), there is flexibility in choosing λ and γ, and some appropriate criterion is required in making that choice. The least squares criterion has been adopted here whereby the sums of squares of residuals obtained by fitting Paris equations to the data for a range of λ, γ combinations are compared. That particular combination yielding the smallest sum of squares then provides the best possible fit of the present model to the data. The (computerised) procedure is as follows:

1. Select λ and γ from the ranges $-1{\cdot}5 \le \lambda \le 0$ and $-2 \le \gamma \le 2$.
2. Calculate ΔK_{eff} for every data point using equations (6), (8) and (12).
3. Fit a Paris equation (9) to the data expressed as log $da\,dN$ versus log ΔK_{eff}, and note the sum of squares of the log $da\,dN$ residuals.
4. Repeat steps 1, 2 and 3 for all λ, γ pairs to determine that pair yielding the minimum residual sum of squares of log $da\,dN$.

* Although the crack growth rate data of Schijve and Hudson have not been derived in an identical manner from the original test data, it is thought unlikely that this fact is of consequence here. Data from different sources are not being compounded.

Examples of the residual sums of squares of log da/dN associated with the regressions* are shown in Figures 7(a), (b) and (c) plotted against X for several values of Z. That particular X, Z combination yielding the minimum sum of squares is noted in each case. It can be seen that for both sets of 2024-T3 data the influence of the shift parameter Z on the residual sum of squares is very much less than that of the stress ratio asymptote X; for the 7075-T6 data the influence of Z is rather more significant – the family of Z curves do not coincide to the same extent in the minimum sum of squares region.

A plot showing the optimum S_{op}/S_{max} versus R curves for the three data sets is shown in Figure 8, and the corresponding transformed crack growth rate data, expressed in terms of ΔK_{eff}, are shown in Figures 9(a), (b) and (c). The least squares fitted straight lines are also shown, along with their equations. The effectiveness of taking R into account in this way is very clear.

Cumulative probability plots of the residuals are shown in Figures 10(a), (b) and (c) using normal ordinates. The plotting position, P_i, used for the ith residual has been determined from

$$P_i = (i - 0{\cdot}5)/r$$

for large r, the total number of data points, after Reference 9. Also shown on the figures are smoothed Kolmogorov-Smirnov 95% confidence bounds based on the given number of data points in each case assumed perfectly normally distributed. Although Figures 9 indicate that the common assumption of normality of log crack growth rate data is not seriously challenged here for the transformed data, the application of the more stringent χ^2 test shows that only the transformed 2024-T3 data of Hudson form an empirical distribution which does not differ significantly from the corresponding normal, Table 2, column 2.

Relevant data associated with the regressions are tabulated in Table 3. Also given there are the results of applying Schijve's equation (5) to the data. The minimum sums of squares are seen to be little higher than those of the present formulations. F tests based on the variance of the residuals for both models show no significant differences for the 2024-T3 data sets; for 7075-T6 however the present formulation is significantly better – the variance ratio becomes significant at the 1% level. Meaningful comparisons of C and n, the Paris constants, are not possible since they operate on different equations ((6), (8) and (12) for the present formulation and (5) and (12) in Schijve's case).

5. CRACK GROWTH PREDICTION

The best fit Paris equations have now been used to predict the crack growth cycles between the successive crack lengths as established on test and given in the original references†. The expectation is, of course, that the predictions will, on average, agree with the data from which they derive. These predictions are shown in Figures 11(a), (b) and (c) expressed in terms of (test cycles/predicted cycles), each between the same two crack lengths, plotted against ΔK_{eff} based upon final interval crack length.

Figures 11 show that, overall, the above expectation is realised. There can be seen however, in all three graphs, very clear indications of a systematic "snaking" trend of the ratio with ΔK_{eff}, and the reason is readily seen from Figure 9. The data points there do, of course, fall in the intermediate section of the overall S shaped or sigmoidal da/dN versus ΔK_{eff} plot. They should, therefore, be even better fitted by an appropriate sigmoidal curve. Points falling below the regression line on Figure 9 become points above unity on Figures 11, and vice versa: the tendency for increased variability at low ΔK_{eff} is no doubt due, at least in part, to inaccuracies

* Preliminary analysis showed that the circled data points in Figures 6(a) and 6(c) were falling into the increasingly steep final region of the sigmoidal crack growth rate curve beyond the central (and nominally linear) region considered here. Those data points have been omitted in further analysis.

† In establishing some of the original crack growth data[10] on 2024-T3 Alclad sheet from which the growth rate data summarised in Reference 7 were based, it was found that the total number of a vs N data points exceeded substantially the total number of derived da/dN data points. This fact accounts for the differing tallies entered on Figures 10(a), and 11(a) and 12(a).

associated with measurements and derivations at shorter crack lengths[11]. Figures 11 show that the test cycles predicted cycles ratio falls, for the most part, between 1·3 and 2.

This same fact may be seen more readily from the cumulative frequency plots of Figure 12 where the ratio very seldom exceeds 2 and is seldom below 1·3. These graphs reflect behaviours similar to their counterparts of Figure 10, although, in the case of Figure 12(c), an increased deviation from the normal takes it outside even the weak Kolmogorov-Smirnov 95% limits. The results of χ^2 tests to check goodness-of-fit with the corresponding normals are similar to those of the data of Figures 10: only the 2024-T3 data of Hudson do not differ significantly from normal, Table 2, column 3. The variance ratio tests listed in Table 4 show that the differences between variability in log crack growth rate and that of log life ratio are not significant for either of the 2024-T3 data sets; for the 7075-T6 data they are, however, significant at the 95% level.

6. CONCLUSIONS

1. The crack opening concept leading to effective, as opposed to nominal, stress intensity ranges in fatigue cycling has provided a sound basis for quantifying the known effect of stress ratio on fatigue crack growth rate. Several existing models have been examined in this Report.

2. A flexible formulation relating crack opening stress ratio with conventional stress ratio (based on a third order polynomial and requiring for its definition two fitted parameters) has been applied to three extensive constant amplitude crack growth rate data sets from the literature (2024-T3 Alclad, 2024-T3 and 7075-T6 sheet materials). Paris equations have been least squares fitted to the log da/dN data expressed in terms of log ΔK_{eff} in each case.

3. Actual growth cycles over given crack length increments fall almost invariably within the range from 1·3 to 2 times those predicted using these equations.

4. The study shows that even better fits would be attainable using, instead of the linear relationship assumed here, the known overall sigmoidal relationship between crack growth rate and effective stress intensity range. This approach is being followed up and should permit realistic extrapolation into the low and high crack growth rate regions beyond those of the present data.

REFERENCES

1. Elber, W. — The Significance of Fatigue Crack Closure. Damage Tolerance in Aircraft Structures. ASTM STP 486, pp. 230-242, 1971.

2. Schijve, J. — Prediction Methods for Fatigue Crack Growth in Aircraft Material. Delft University of Technology Report LR-282, June 1979.

3. Bell, P. D.; Creager, M. — Crack Growth Analysis for Arbitrary Spectrum Loading. AFFDL-TR-74-129, 1974.

4. Bell, P. D.; Wolfman, A. — Mathematical Modelling of Crack Growth Interaction Effects. Fatigue Crack Growth under Spectrum Loads. ASTM STP 595, pp. 157-171, 1976.

5. Fidnoff, H. L.; Bell, P. D. — Application of the Crack Closure Concept to Aircraft Fatigue Crack Propagation Analysis. Fatigue Life of Structures under Operational Loads. Proceedings of the 9th ICAF Symposium, Darmstadt, 1977.

6. Newman, J. C. — A Finite Element Analysis of Fatigue Crack Closure. Mechanics of Crack Growth, ASTM STP 590, pp. 281-301, 1976.

7. Schijve, J. — The Stress Ratio Effect on Fatigue Crack Growth in 2024-T3 Alclad and the Relation to Crack Closure. Technische Hogeschool Delft, Memorandum M-336, August 1979.

8. Hudson, C. M. — Effect of Stress Ratio on Fatigue Crack Growth in 7075-T6 and 2024-T3 Aluminum-Alloy Specimens. NASA Technical Note TN D-5390, August 1969.

9. Shimokawa, T. — A New Plotting Method to Estimate the Population Parameters of the Normal Distribution. National Aerospace Laboratory (Japan) Technical Report TR-464T, November 1977.

10. Ewalds, H. L. — The Effect of Stress Ratio and Maximum Stress on Fatigue Crack Propagation in 2024-T3 Alclad Sheet Material. Delft University of Technology, Metallurgical Department Report AM37601, June 1976.

11. Jost, G. S.; Esson, G. P. — Fatigue of D6ac Steel Specimens - Means and Variabilities under Programmed Loading. Aeronautical Research Laboratories Report ARL SM 349, April 1974.

12. de Koning, A. U. — A Simple Crack Closure Model for Prediction of Fatigue Crack Growth Rates under Variable Amplitude Loading. NLR Report MP80006U, January 1980.

13. Schijve, J. — Some Formulas for the Crack Opening Stress Level. Technische Hogeschool Delft, Memorandum M-368, April 1980.

TABLE 1

Eidinoff and Bell's Equation, Ref. 5

$$S_{op}/S_{max} = (S_{op}/S_{max})_1 - [(S_{op}/S_{max})_0 - (S_{op}/S_{max})_1](1 - R)^P$$

Material	$(S_{op}/S_{max})_1$	$(S_{op}/S_{max})_0$	P
Ti-6Al-4V (EBWeld) Ti-6Al-4V (STA) Ti-6Al-4V (Annealed)	0·332	0·400	3·33
2219 T851 2024 T851	0·347	0·400	3·93
2024 T3	0·450	0·500	3·42
7075 T651	0·450	0·500	3·62

These equations are plotted in Figure 2.

TABLE 2

Summary of χ^2 Tests on log Crack Growth Rate Residuals and log Life ratios

Data Source	Residuals (Figs 10)	Ratios (Figs 12)
Schijve 2024-T3 Alclad	36·4	21·6
Hudson 2024-T3	3·2	5·2
Hudson 7075-T6	22·7	70·1

$95\%\ \chi^2_3$ 2·17

$5\%\ \chi^2_3$ 14·07

TABLE 3

Least Squares Fitted Paris Equations

Data			Present Formulation (eq. 6, 8, 12)						Schijve (eq. 5, 12)				Significance Tests†		
Material	Ref.	No. of Data Points	Min. SS*	St. Dev.	X	Z	C ($\times 10^{-3}$)	n	Min. SS*	St. Dev.	C 10^{-3}	n	S_1^2 / S_2^2	5% F	1% F
2024-T3 Alclad	7	423	9·41	0·149	0·62	0·71	8·25	3·530	9·74	0·152	0·114	3·538	1·034	1·174	1·255
2024-T3	8	210	4·77	0·151	1·09	0·16	8·19	3·654	5·69	0·165	7·52	3·744	1·193	1·257	1·382
7075-T6	8	409	7·50	0·136	0·68	1·14	0·614	3·764	10·91	0·164	0·266	3·571	1·456	1·177	1·260

* Minimum sum of squares of log da/dN about regression line

† S_1^2 – Schijve variance

S_2^2 – Variance of present formulation.

TABLE 4

Variance Ratio Tests on log Growth Rate and log Life Ratio Data

Data	2024-T3 Alclad (Schijve)		2024-T3 (Hudson)		7075-T6 (Hudson)	
	S	r	S	r	S	r
Log (test life predicted life)	0·1604	672*	0·1534	208	0·1511	407
log (da/dN)	0·1494	421*	0·1510	208	0·1356	407
$(S_1/S_2)^2$	1·153		1·032		1·242	
5% F_{r_1, r_2}	1·154		1·257		1·177	
1% F_{r_1, r_2}					1·260	
Significance	N.S.		N.S.		Sig.	

* See footnote, Section 5.

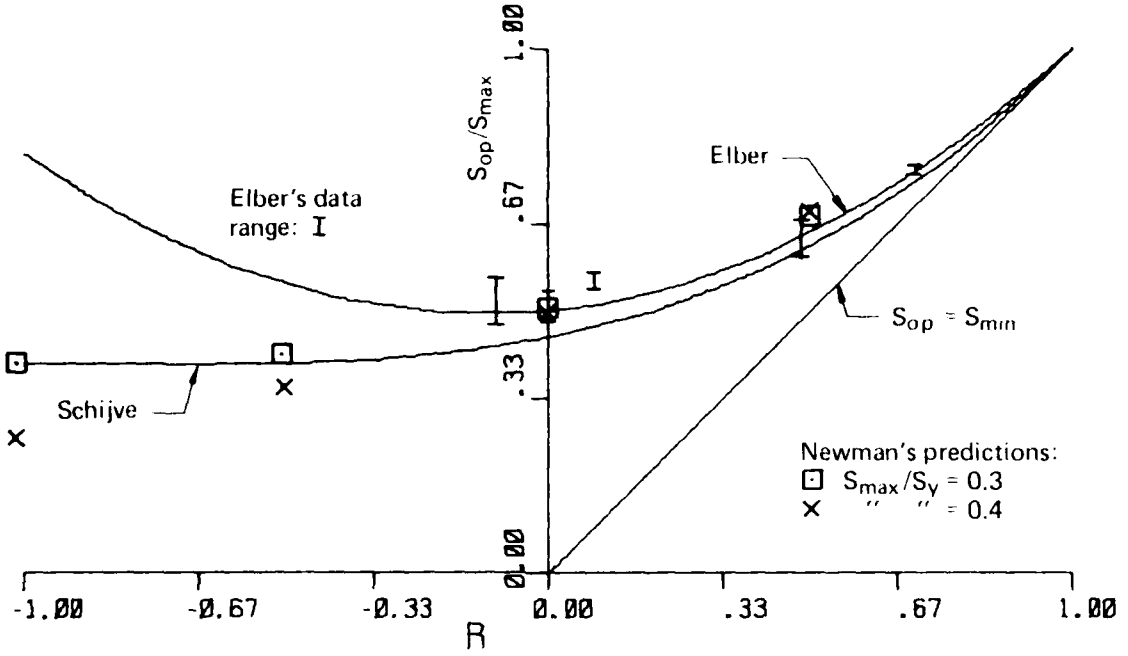

FIG. 1 ELBER'S AND SCHIJVE'S EQUATIONS, ELBER'S DATA, NEWMAN'S PREDICTIONS

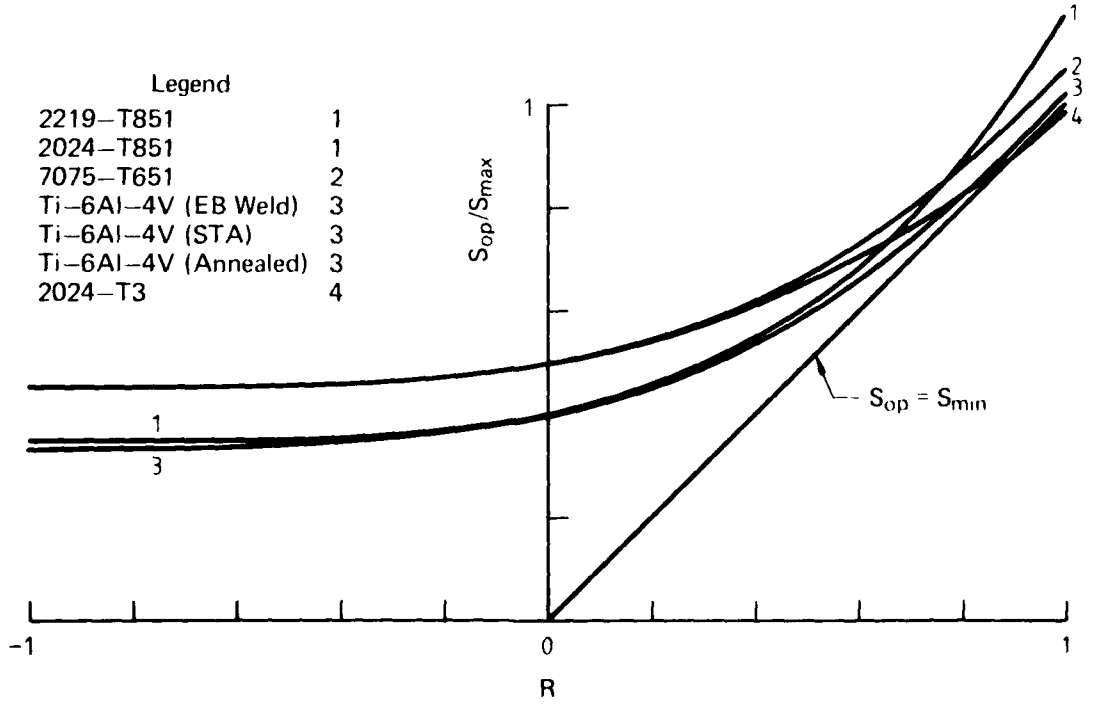

FIG. 2 EIDINOFF AND BELL'S EQUATIONS FOR FOUR ALUMINIUM AND THREE TITANIUM ALLOYS

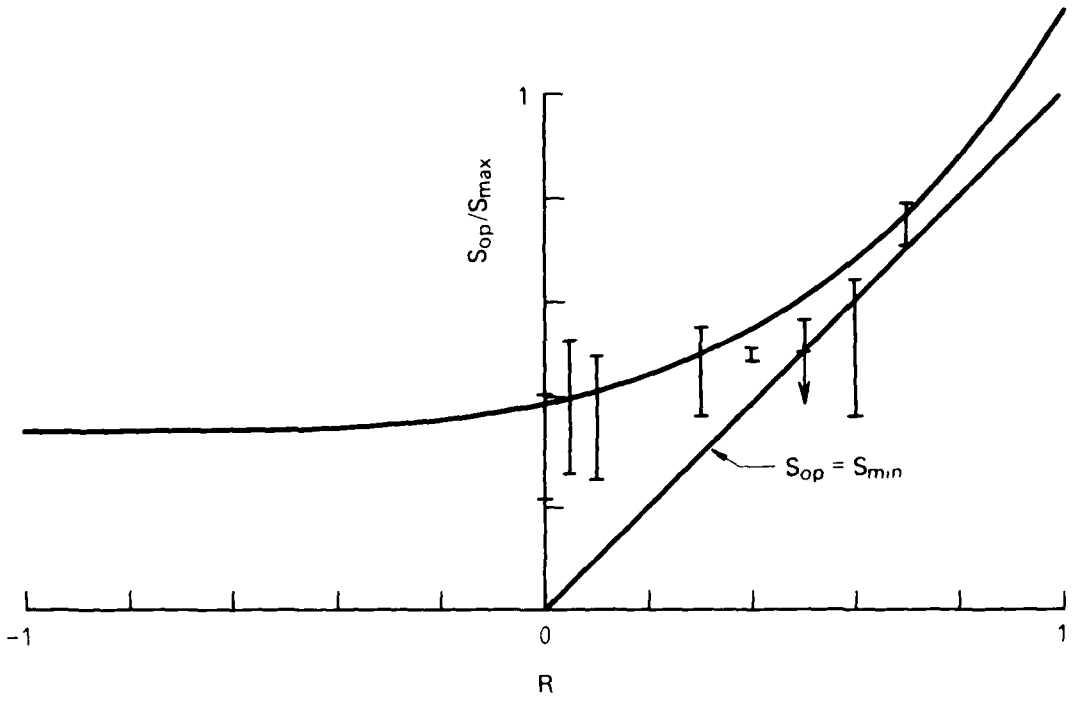

FIG. 3 EIDINOFF AND BELL'S EQUATION FOR 2219–T851 ALUMINIUM ALLOY, AND MEASURED DATA RANGES

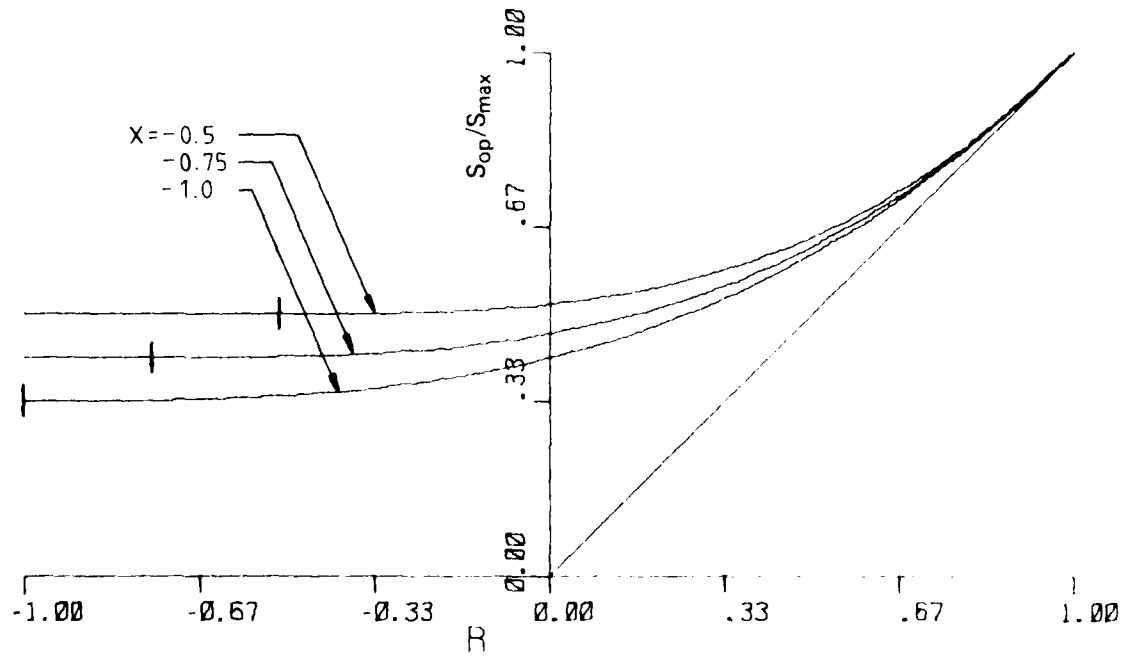

FIG. 4 FAMILY OF CURVES, eq (6)

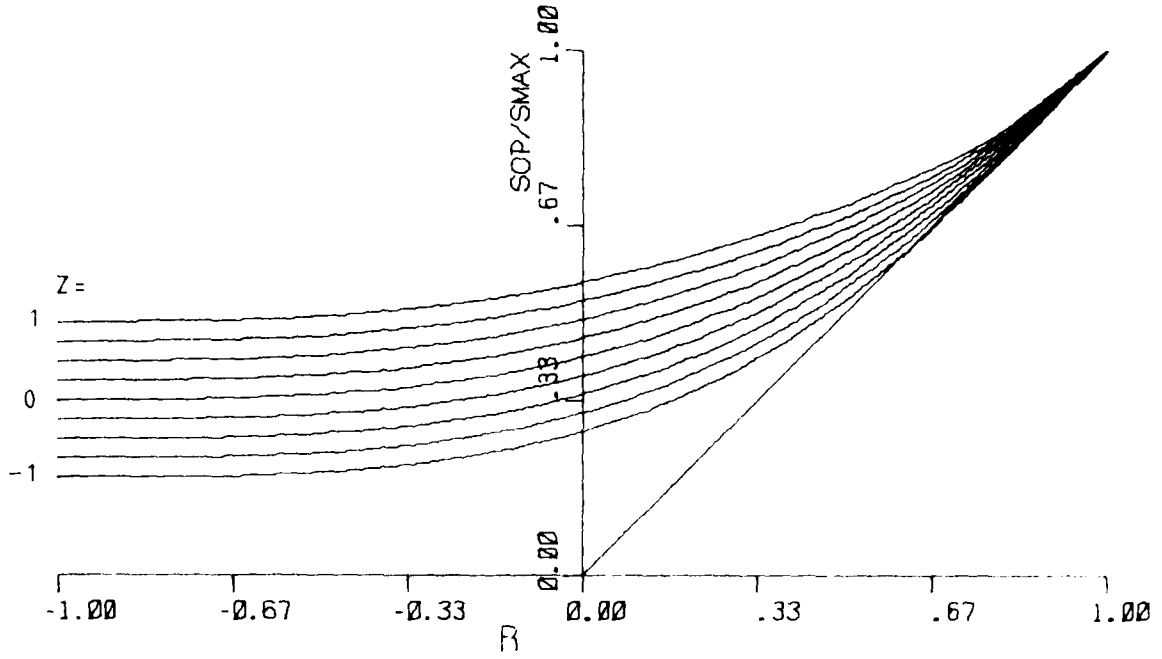

FIG. 5(a) FAMILY OF CURVES, eqs (6) AND (8), X = −1

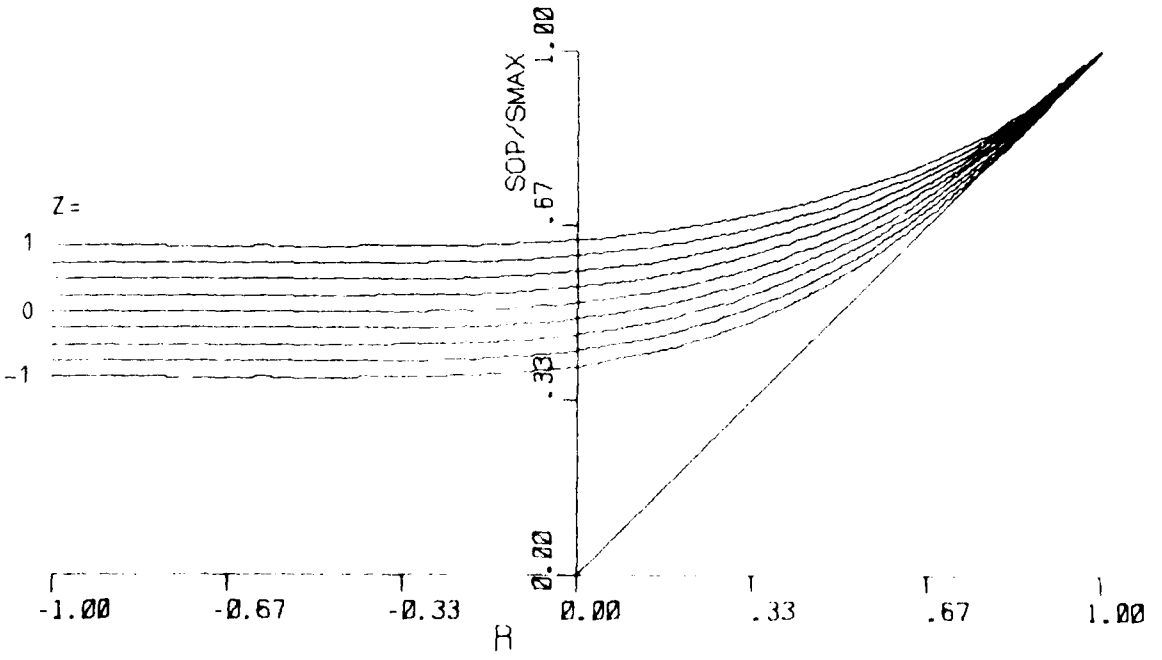

FIG. 5(b) FAMILY OF CURVES, eqs (6) AND (8), X = −0.5

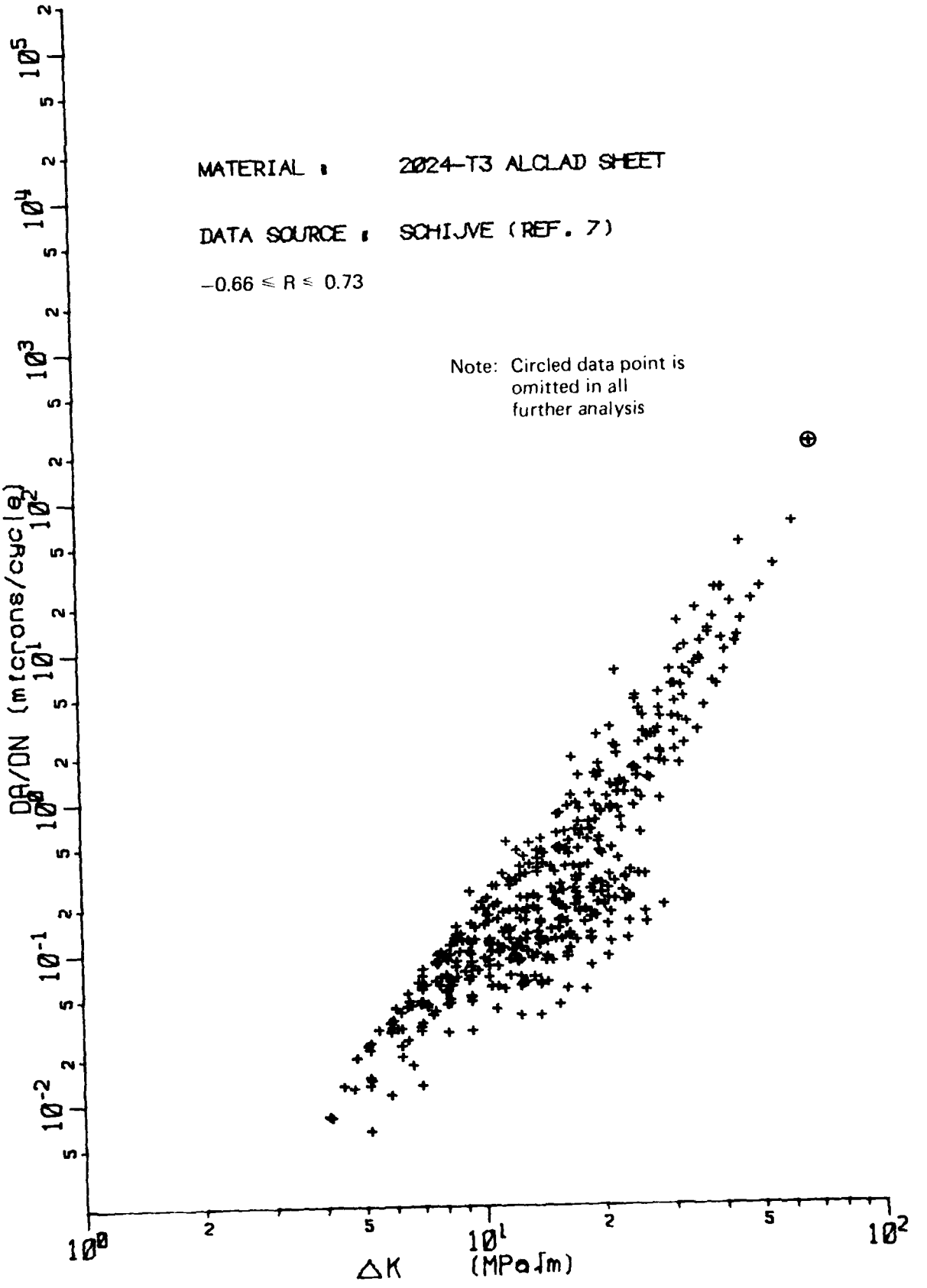

FIG. 6(a) CRACK GROWTH DATA : 2024-T3 ALCLAD SHEET

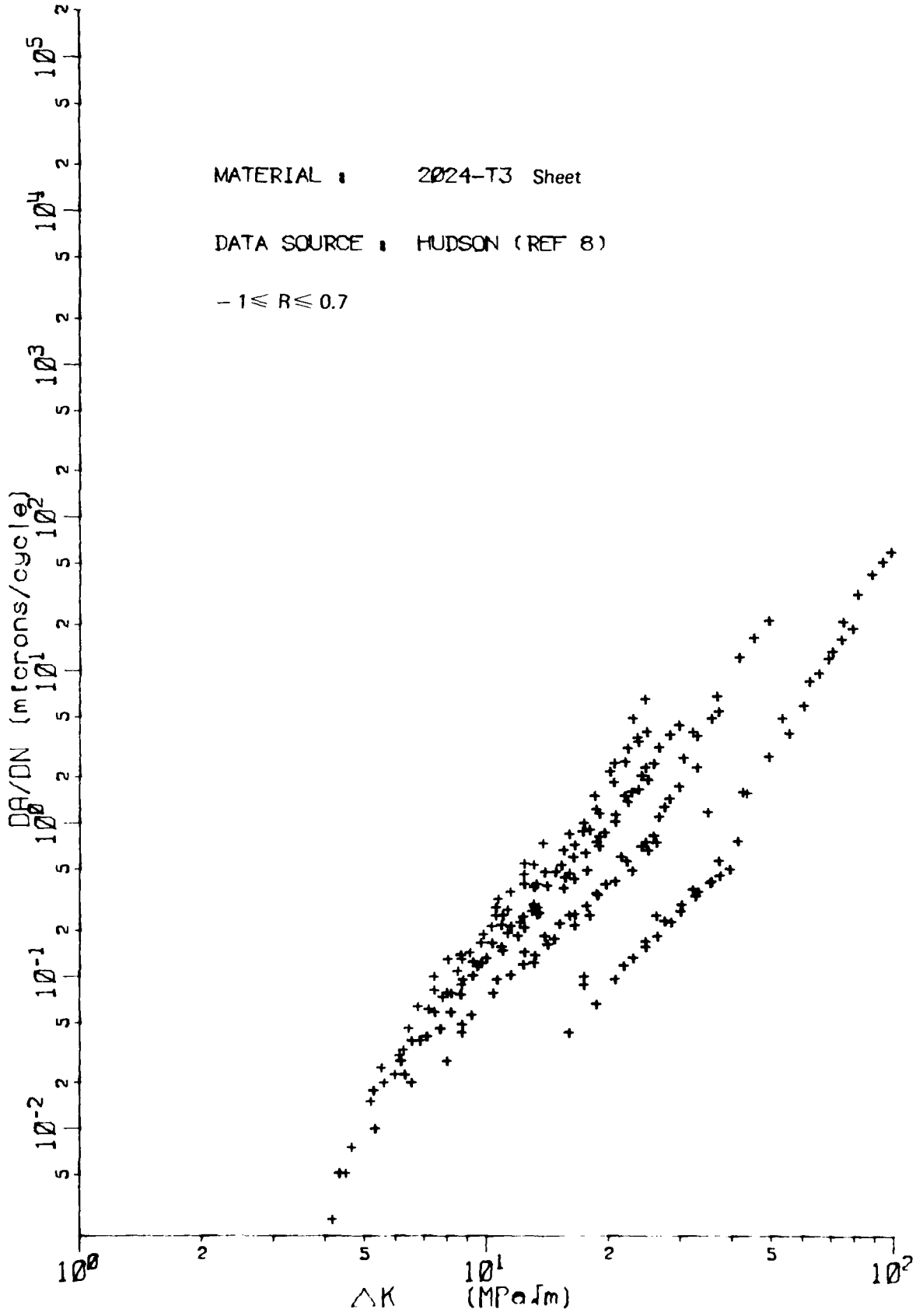

FIG. 6(b) CRACK GROWTH DATA : 2024-T3 SHEET

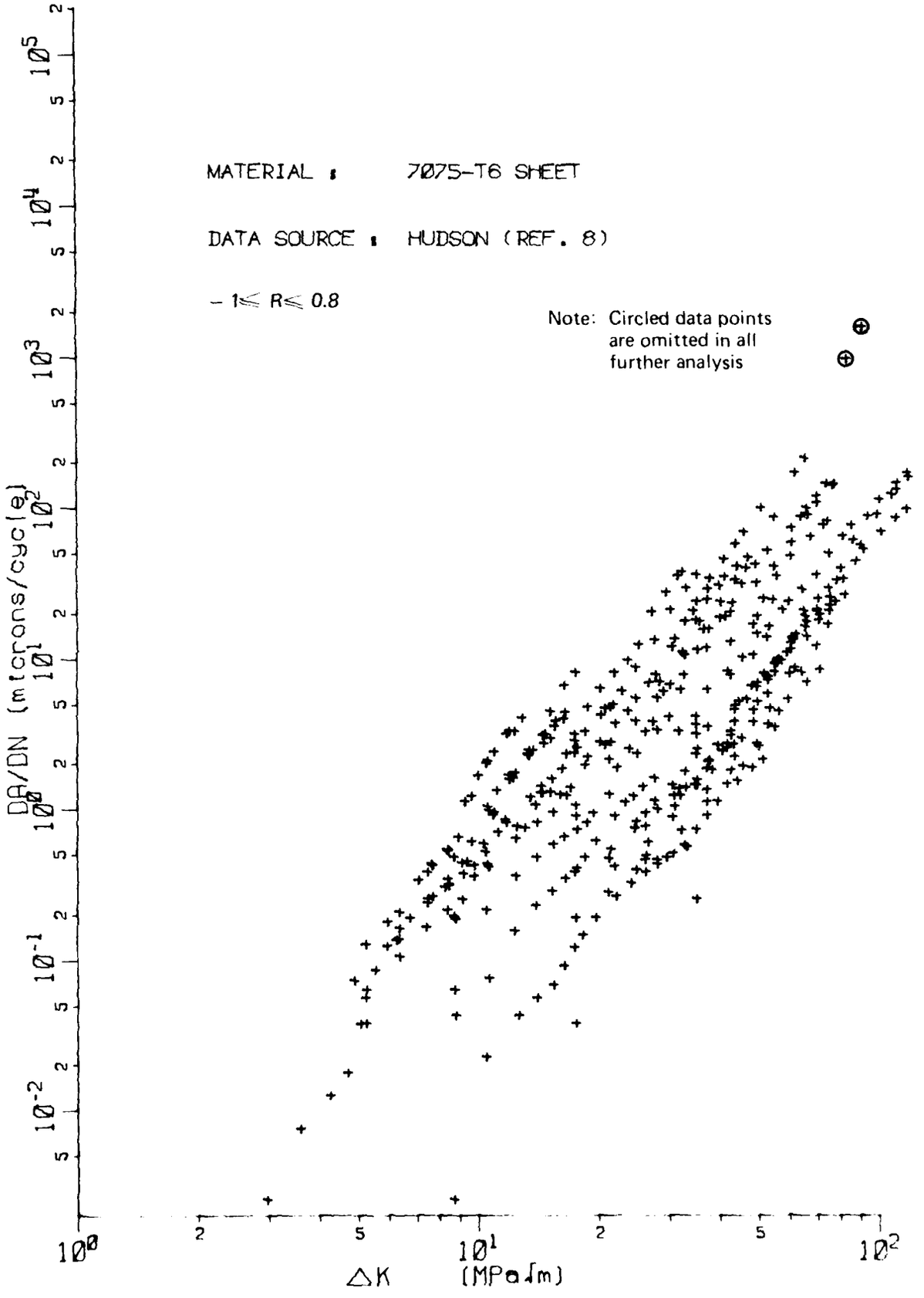

FIG. 6(c) CRACK GROWTH DATA : 7075-T6 SHEET

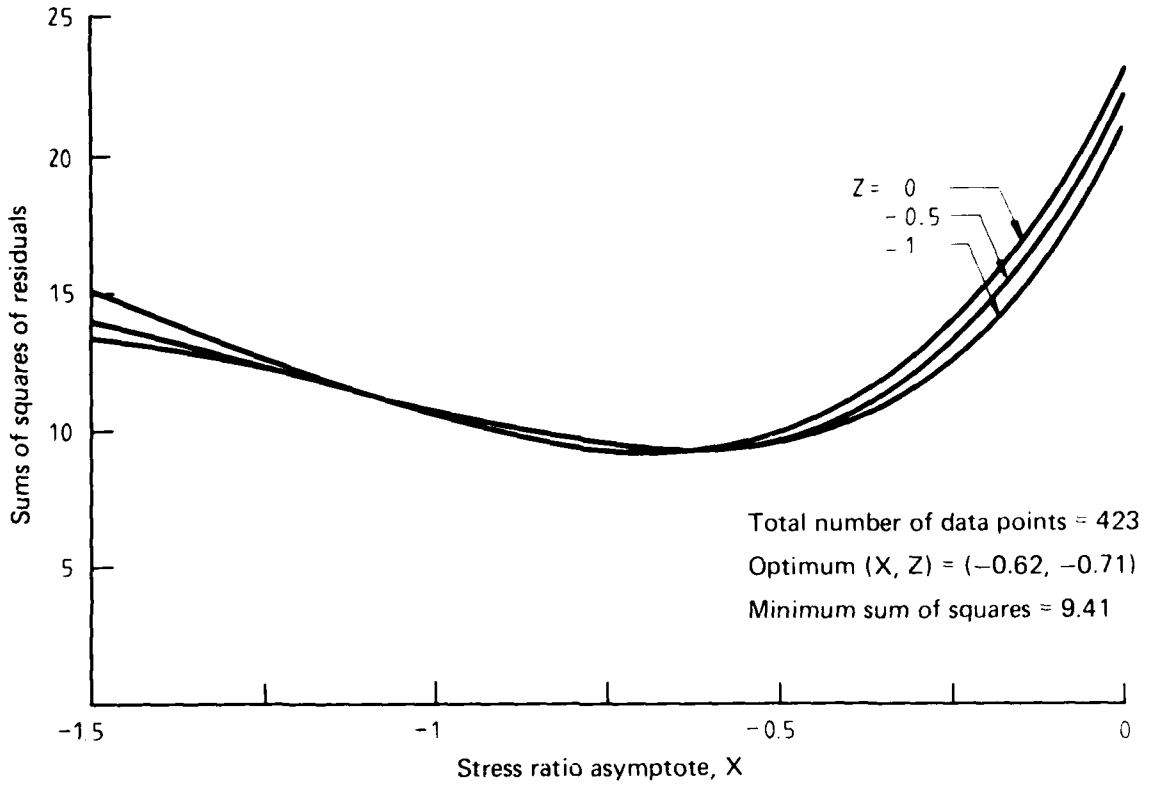

FIG. 7(a) ERROR SUMS OF SQUARES FOR 2024–T3 ALCLAD SHEET (SCHIJVE, REF. 7)

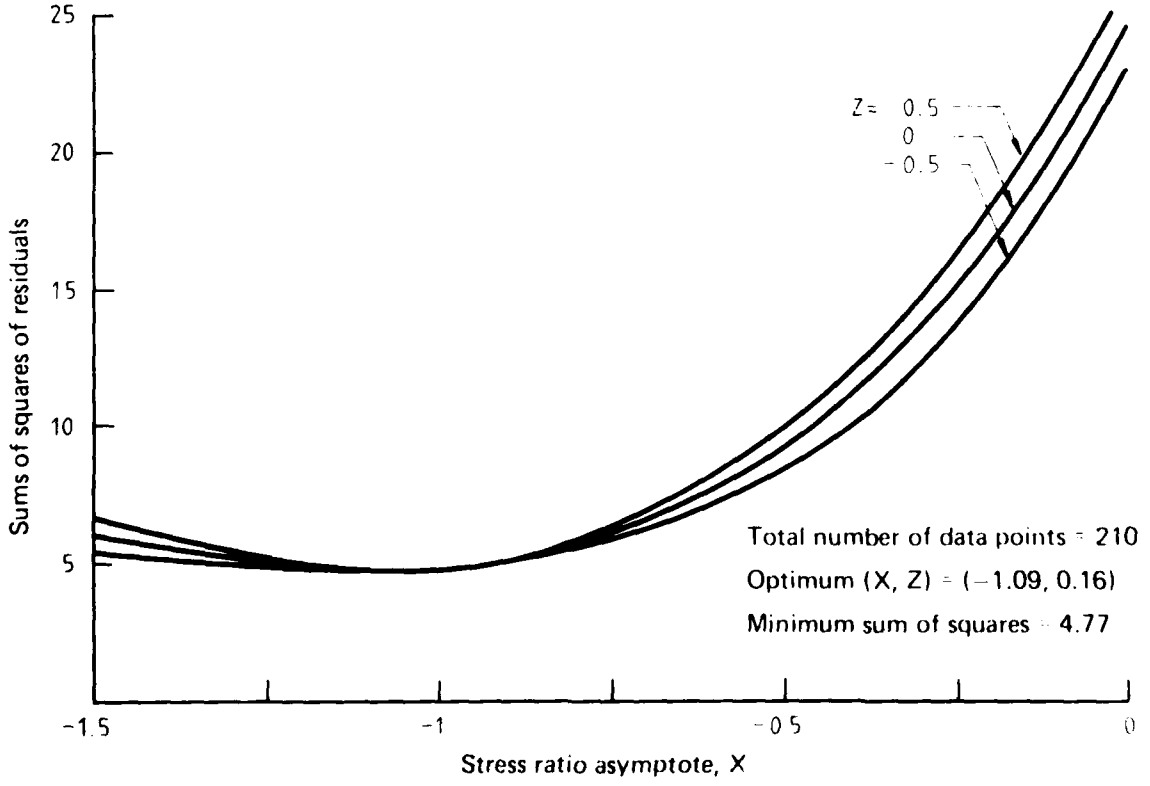

FIG. 7(b) ERROR SUMS OF SQUARES FOR 2024–T3 SHEET (HUDSON, REF 7)

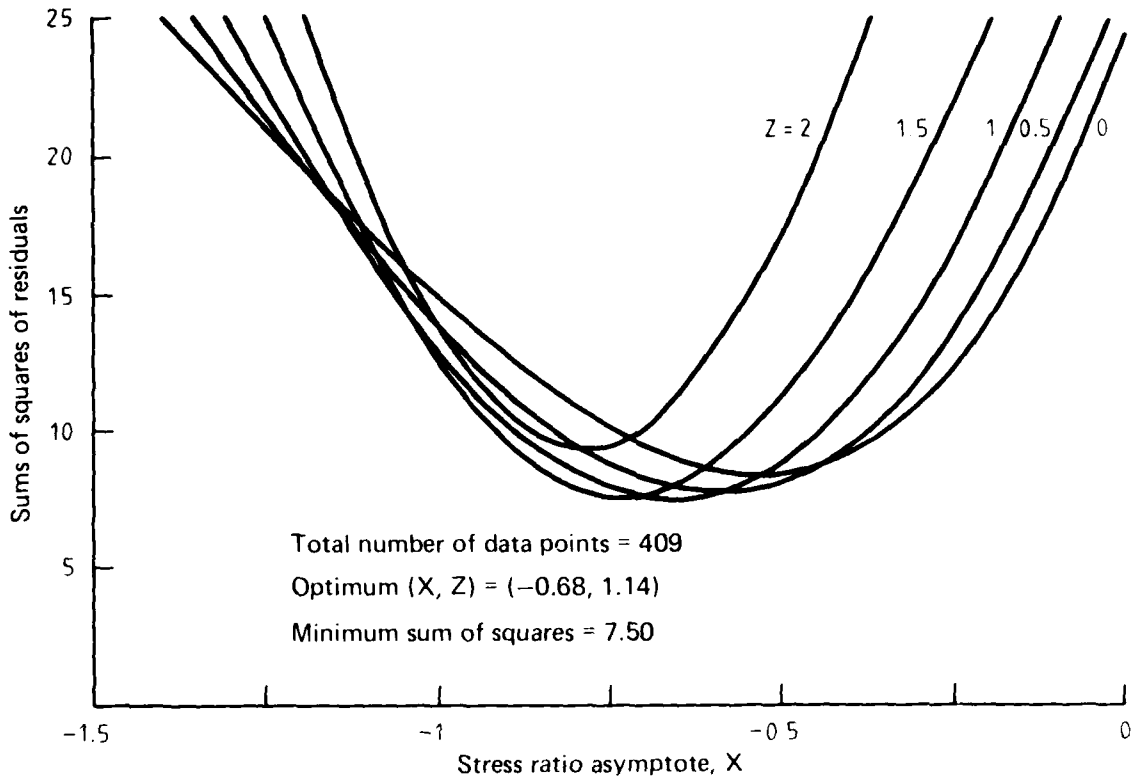

FIG. 7(c) ERROR SUMS OF SQUARES FOR 7075–T6 SHEET (HUDSON, REF 8)

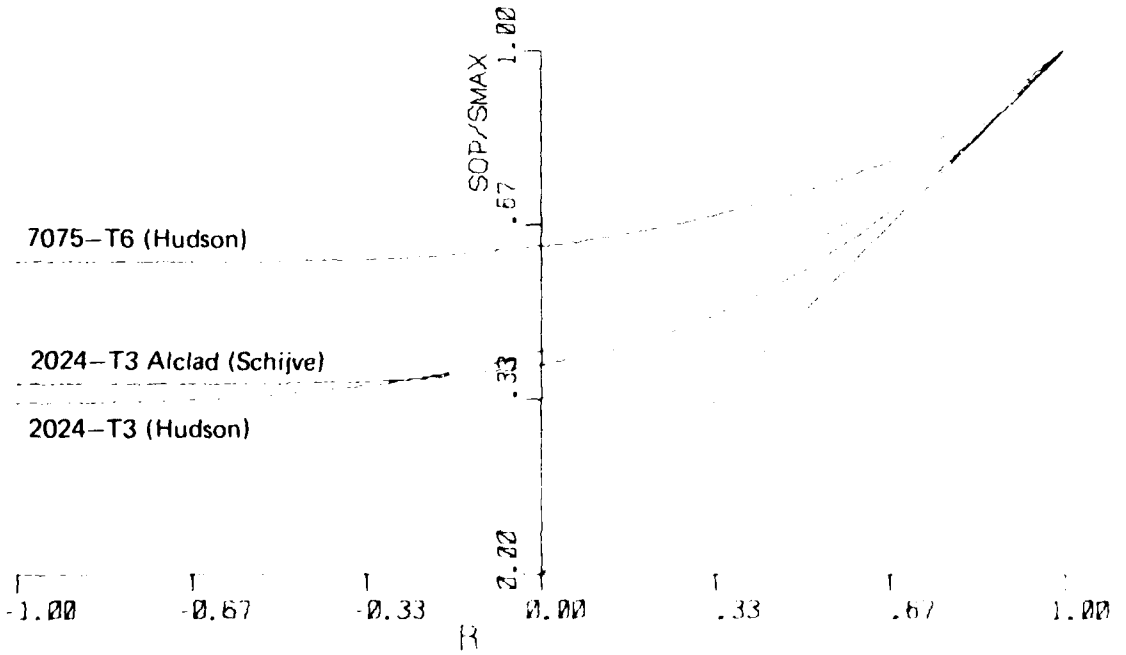

FIG. 8 BEST FIT CRACK OPENING RELATIONSHIPS FOR THREE DATA SETS

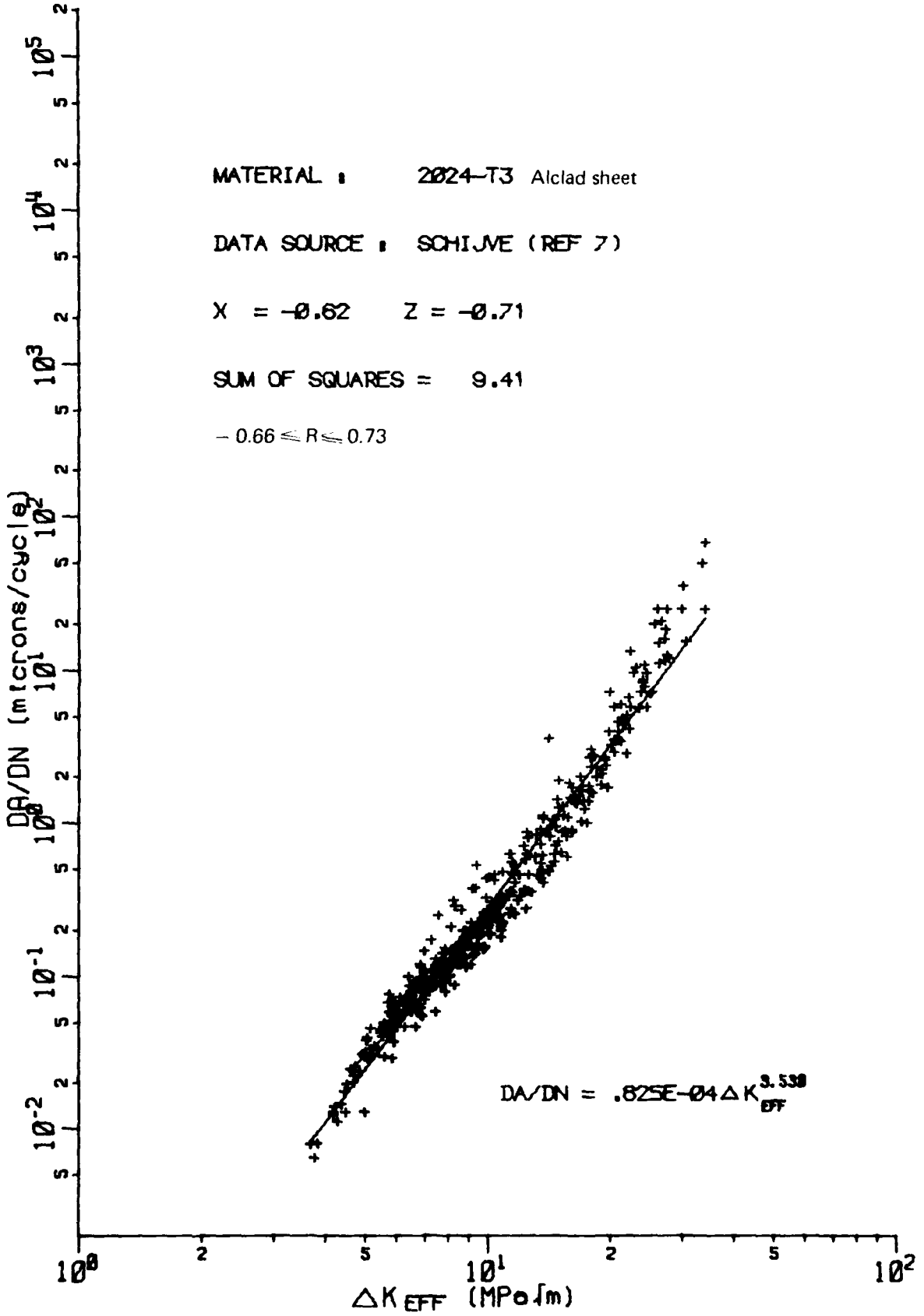

FIG. 9(a) TRANSFORMED CRACK GROWTH DATA : 2024-T3 ALCLAD SHEET

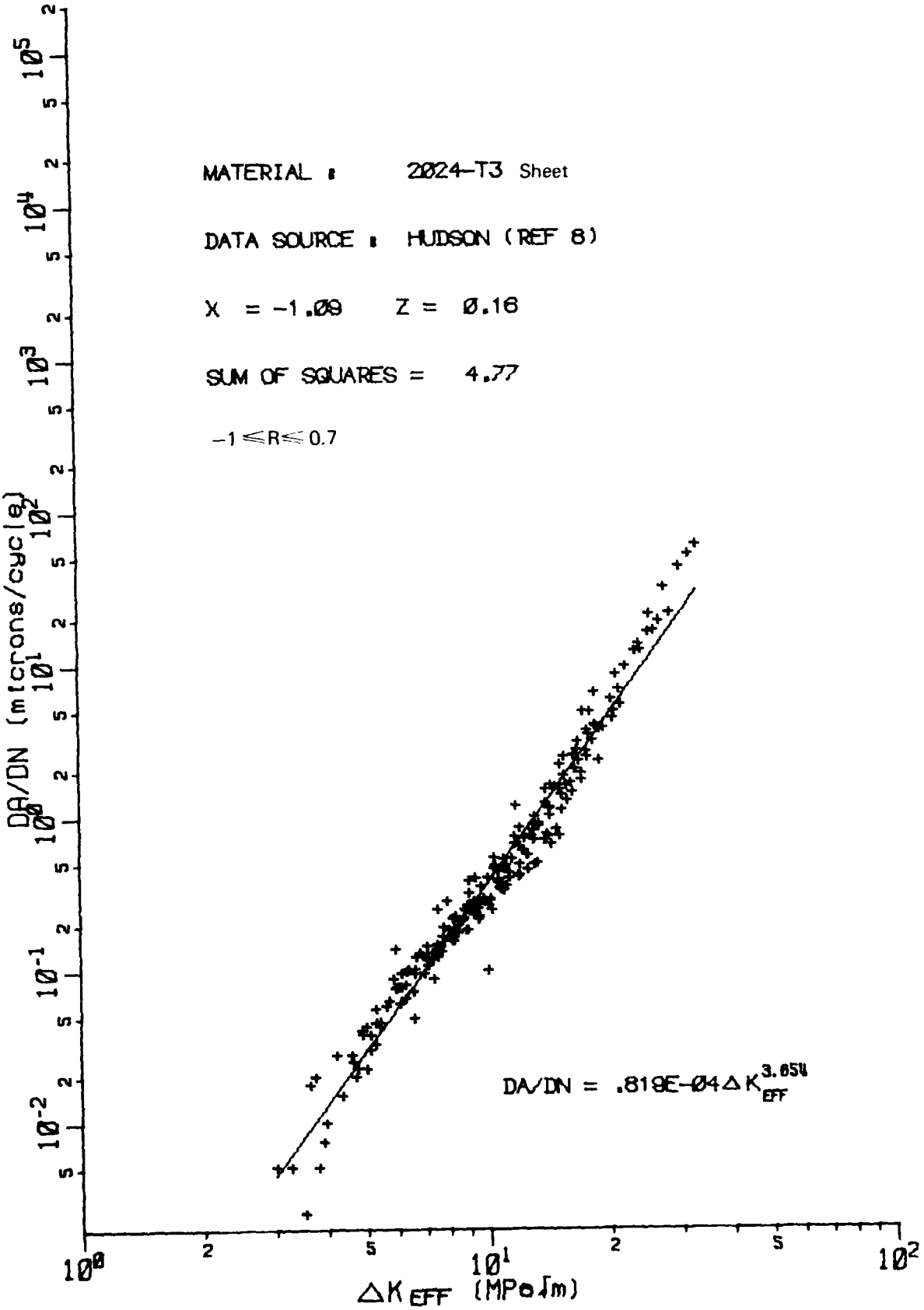

FIG. 9(b) TRANSFORMED CRACK GROWTH DATA : 2024-T3 SHEET

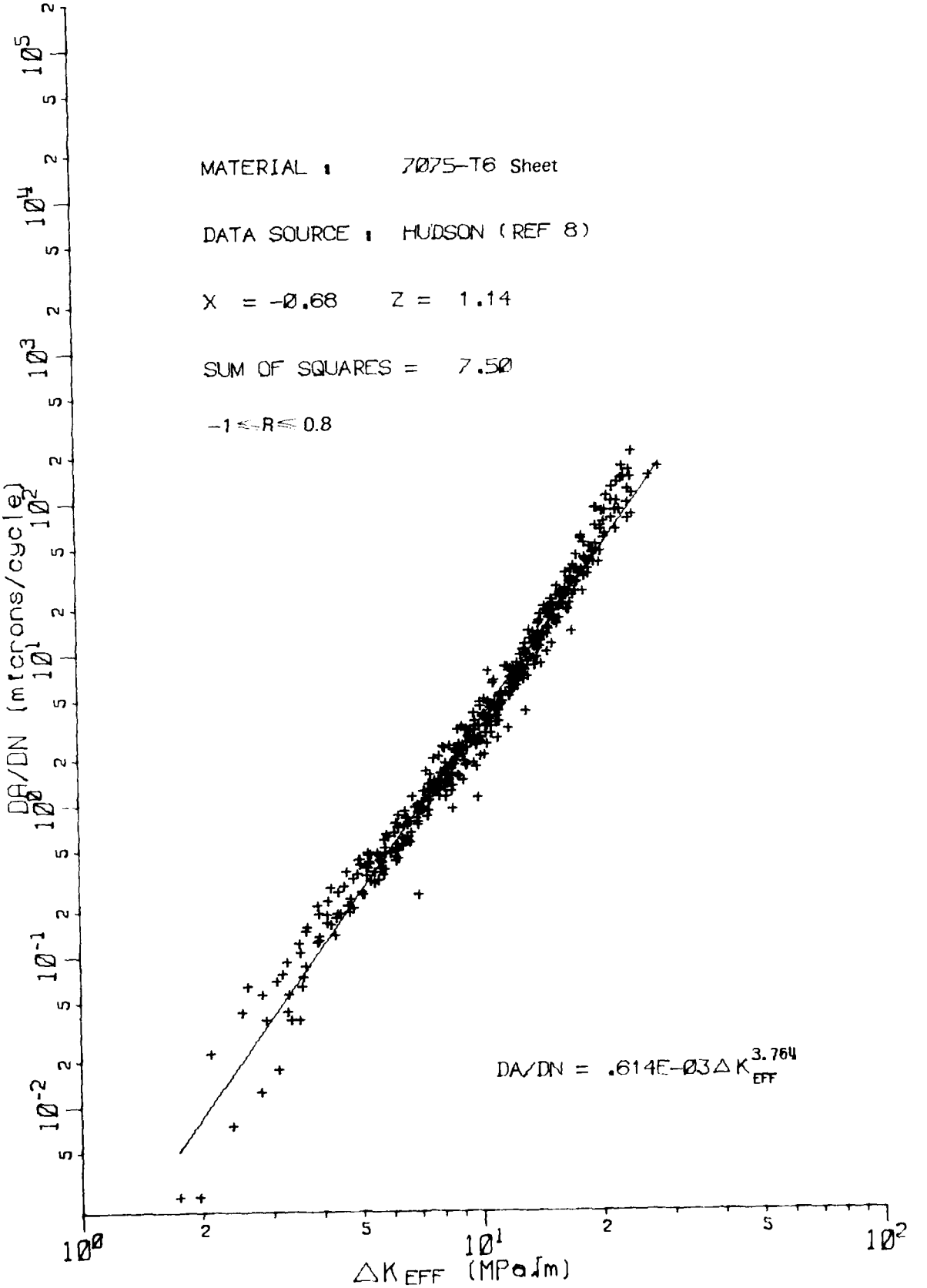

FIG. 9(c) TRANSFORMED CRACK GROWTH DATA : 7075-T6 SHEET

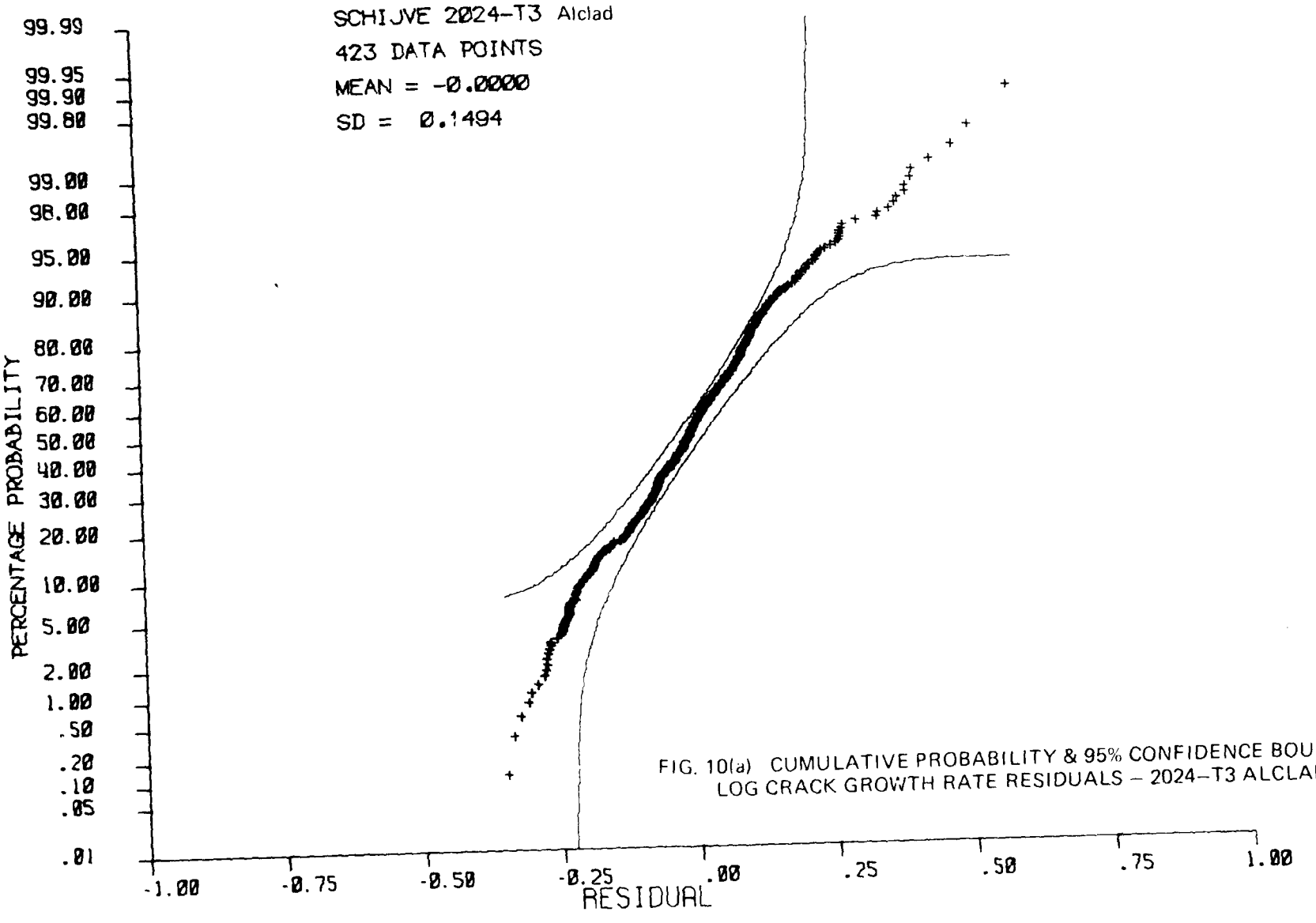

FIG. 10(a) CUMULATIVE PROBABILITY & 95% CONFIDENCE BOUNDS OF LOG CRACK GROWTH RATE RESIDUALS – 2024-T3 ALCLAD

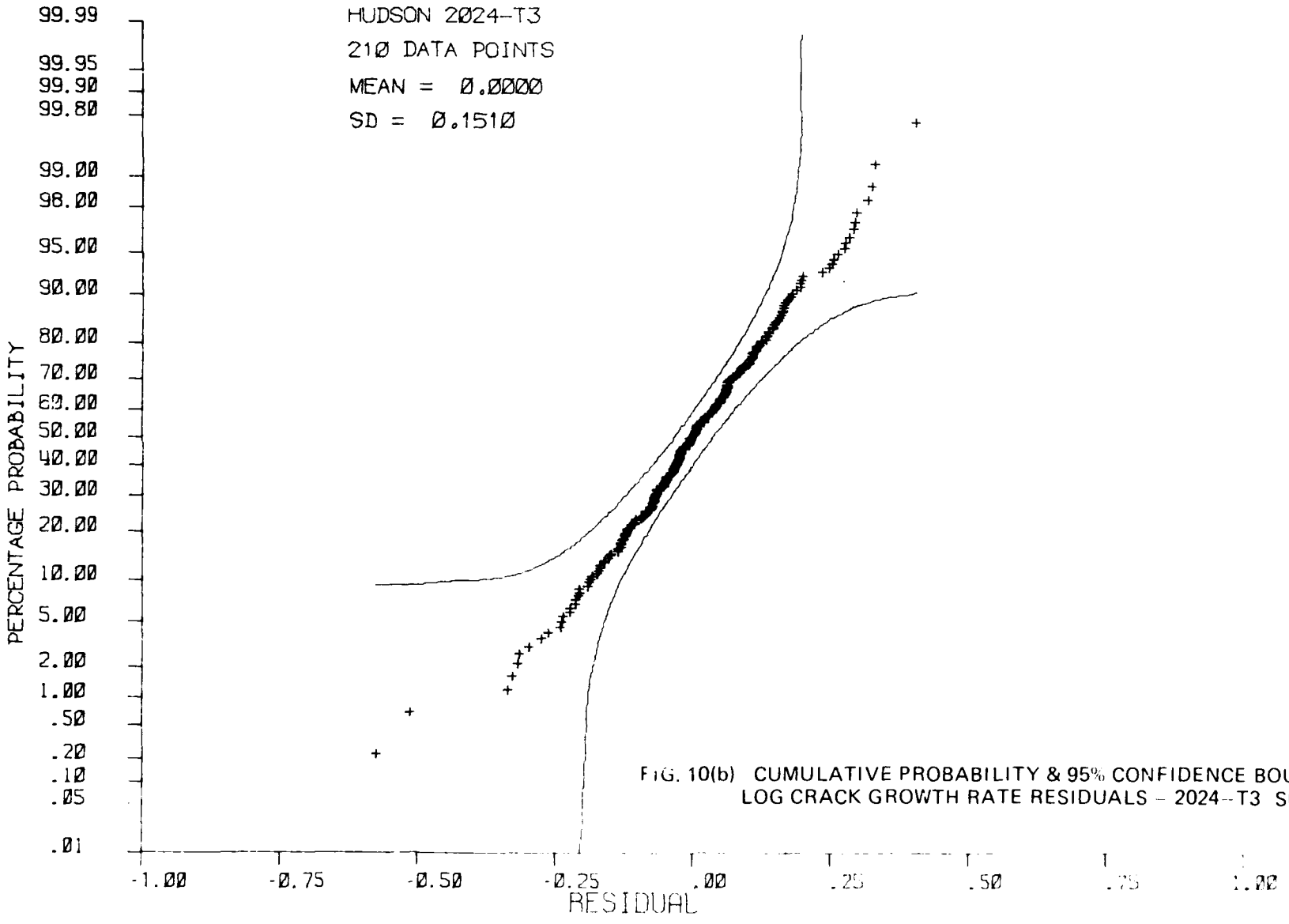

FIG. 10(b) CUMULATIVE PROBABILITY & 95% CONFIDENCE BOUNDS OF LOG CRACK GROWTH RATE RESIDUALS – 2024–T3 SHEET

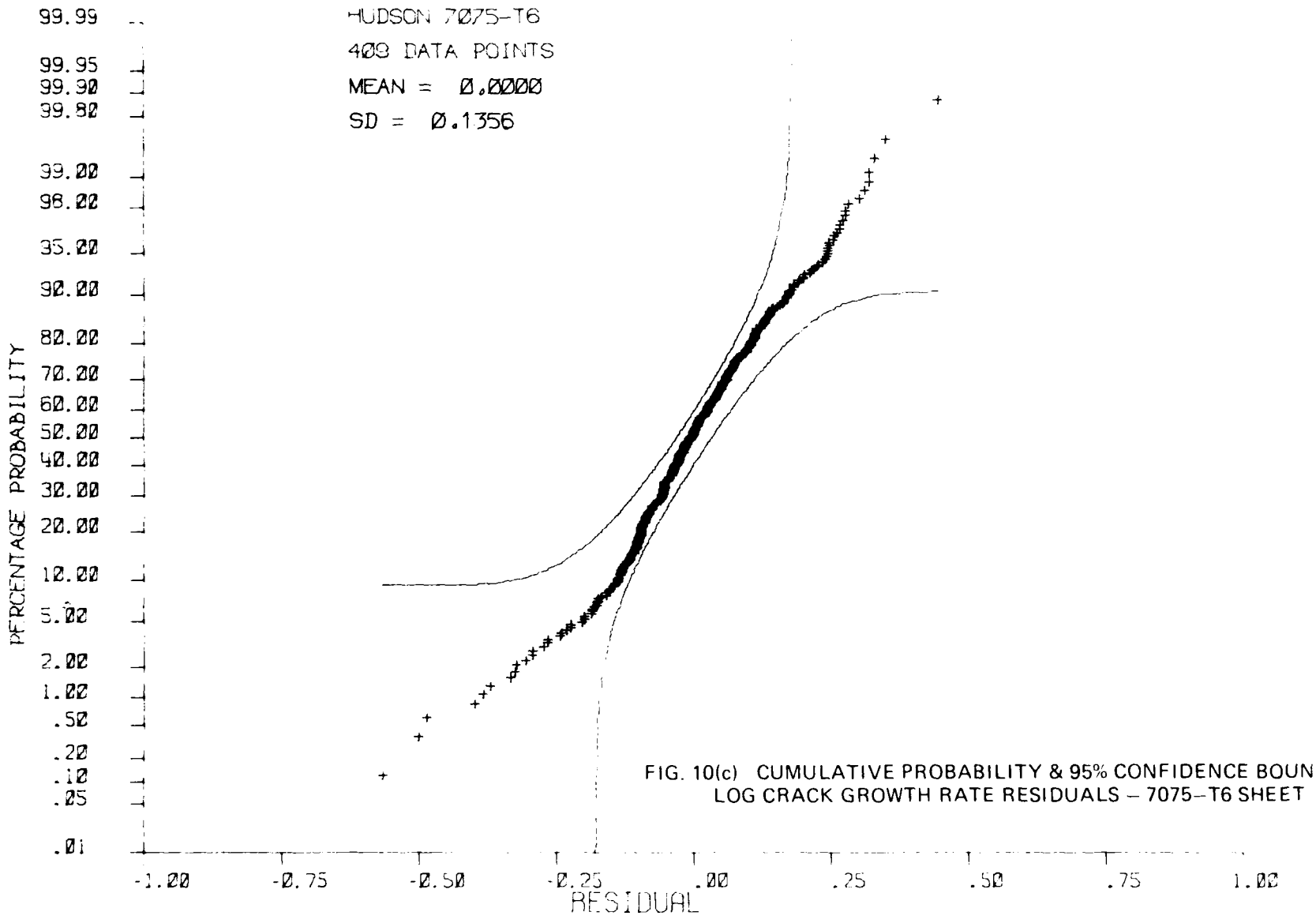

FIG. 10(c) CUMULATIVE PROBABILITY & 95% CONFIDENCE BOUNDS OF LOG CRACK GROWTH RATE RESIDUALS – 7075–T6 SHEET

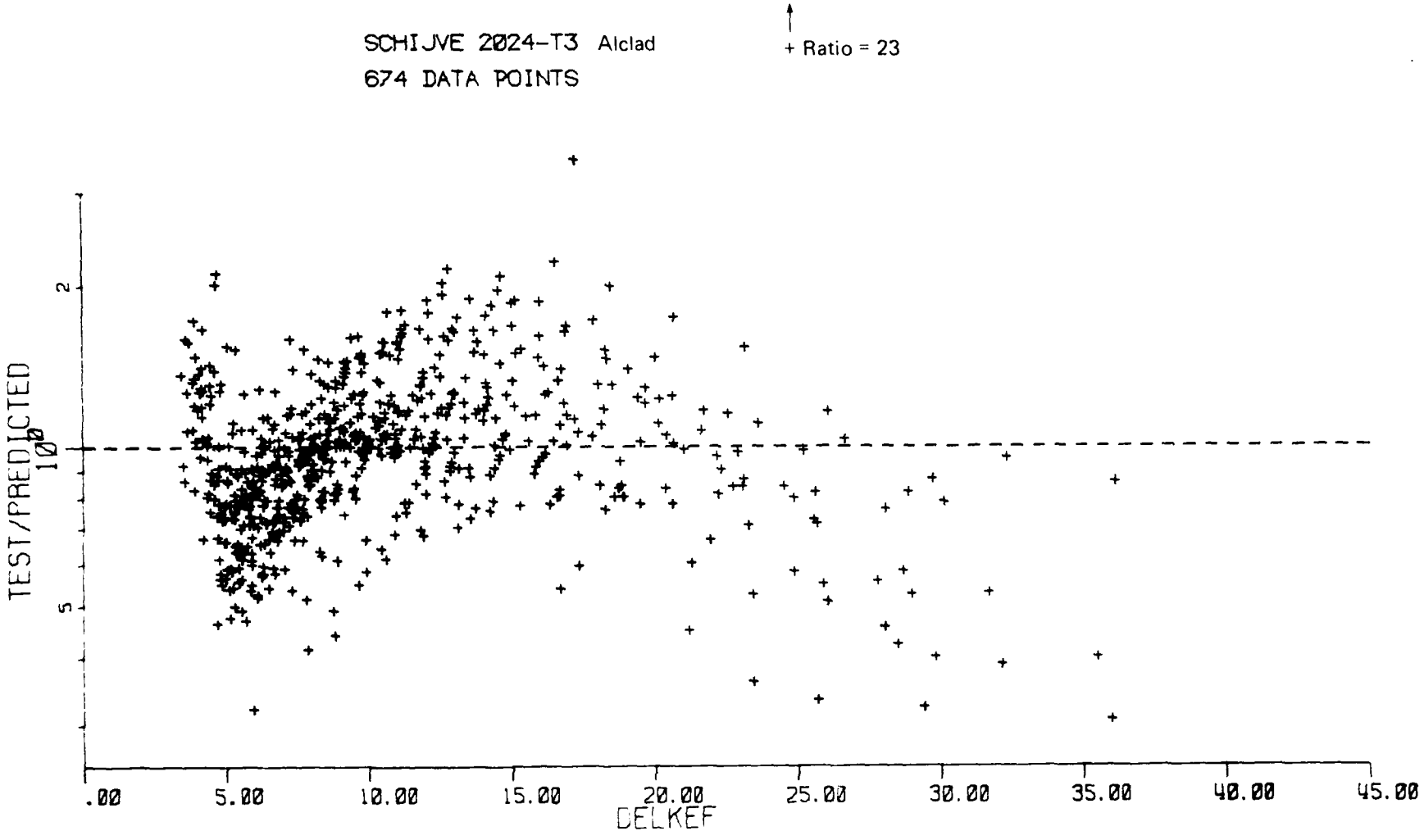

FIG. 11(a) RATIO OF TEST CRACK GROWTH CYCLES TO THOSE PREDICTED VERSUS EFFECTIVE STRESS INTENSITY RANGE – 2024–T3 ALCLAD SHEET

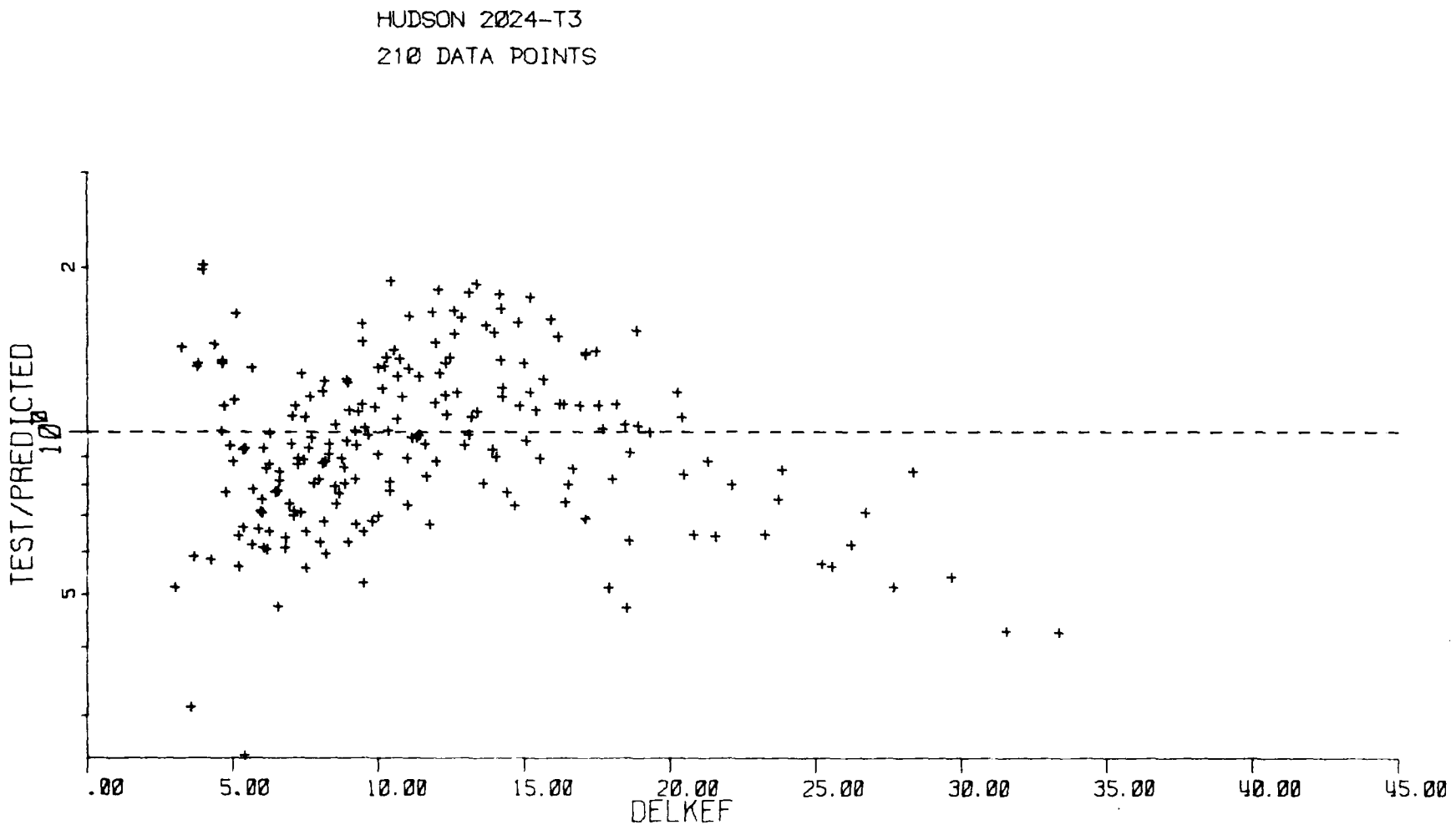

FIG. 11(b) RATIO OF TEST CRACK GROWTH CYCLES TO THOSE PREDICTED VERSUS EFFECTIVE STRESS INTENSITY RANGE – 2024-T3 SHEET

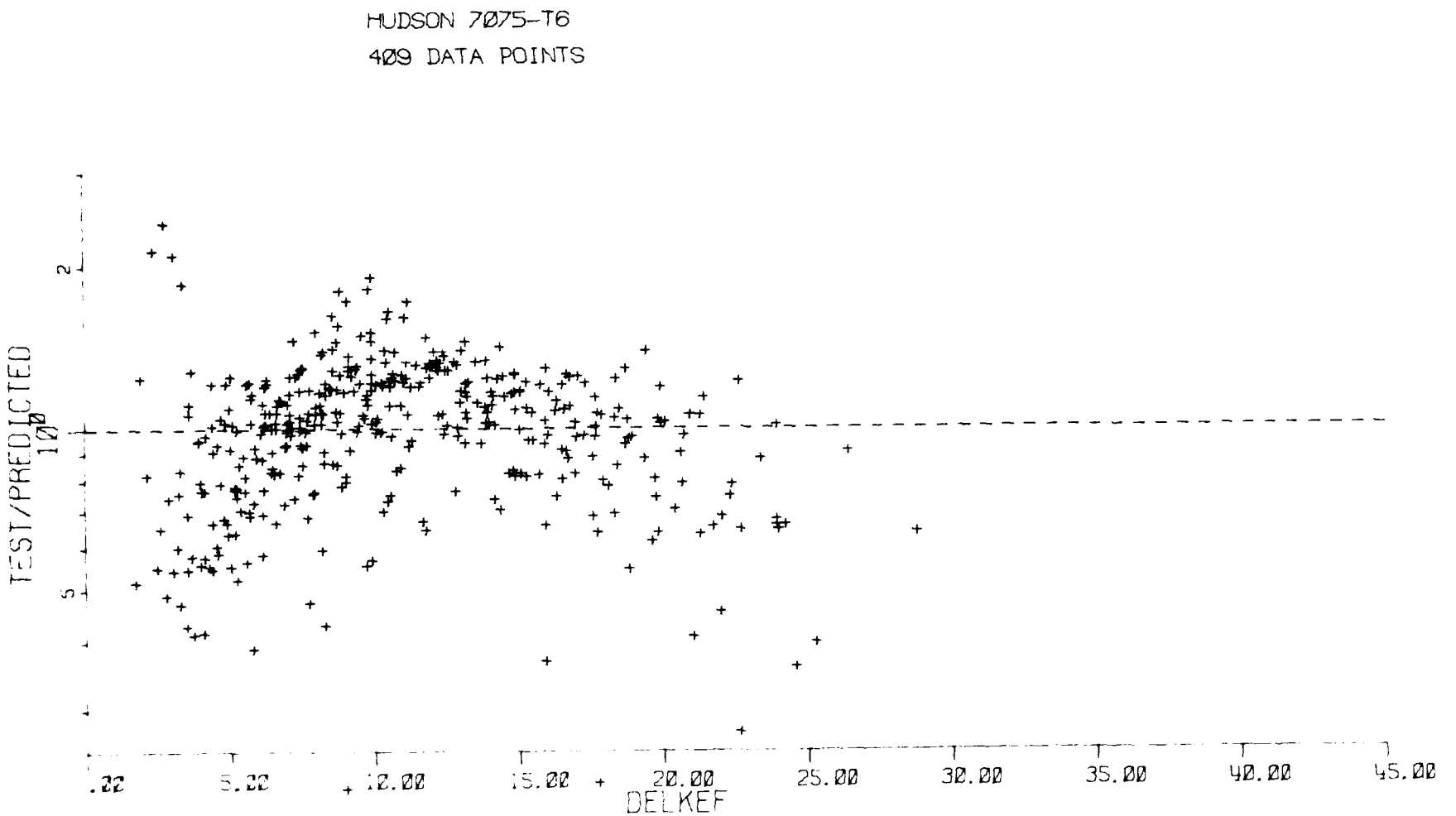

FIG. 11(c) RATIO OF TEST CRACK GROWTH CYCLES TO THOSE PREDICTED VERSUS EFFECTIVE STRESS INTENSITY RANGE – 7075–T6 SHEET

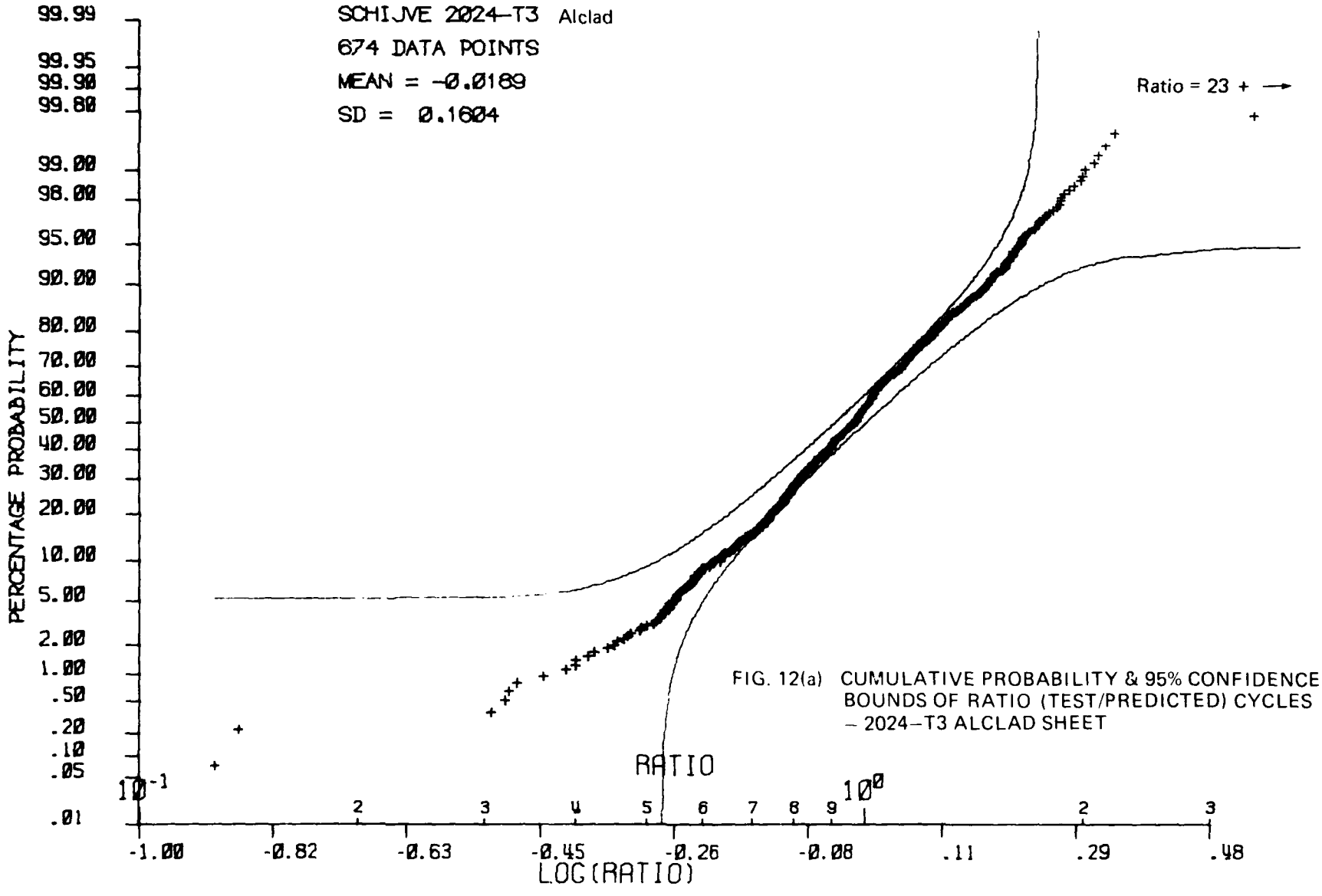

FIG. 12(a) CUMULATIVE PROBABILITY & 95% CONFIDENCE BOUNDS OF RATIO (TEST/PREDICTED) CYCLES – 2024-T3 ALCLAD SHEET

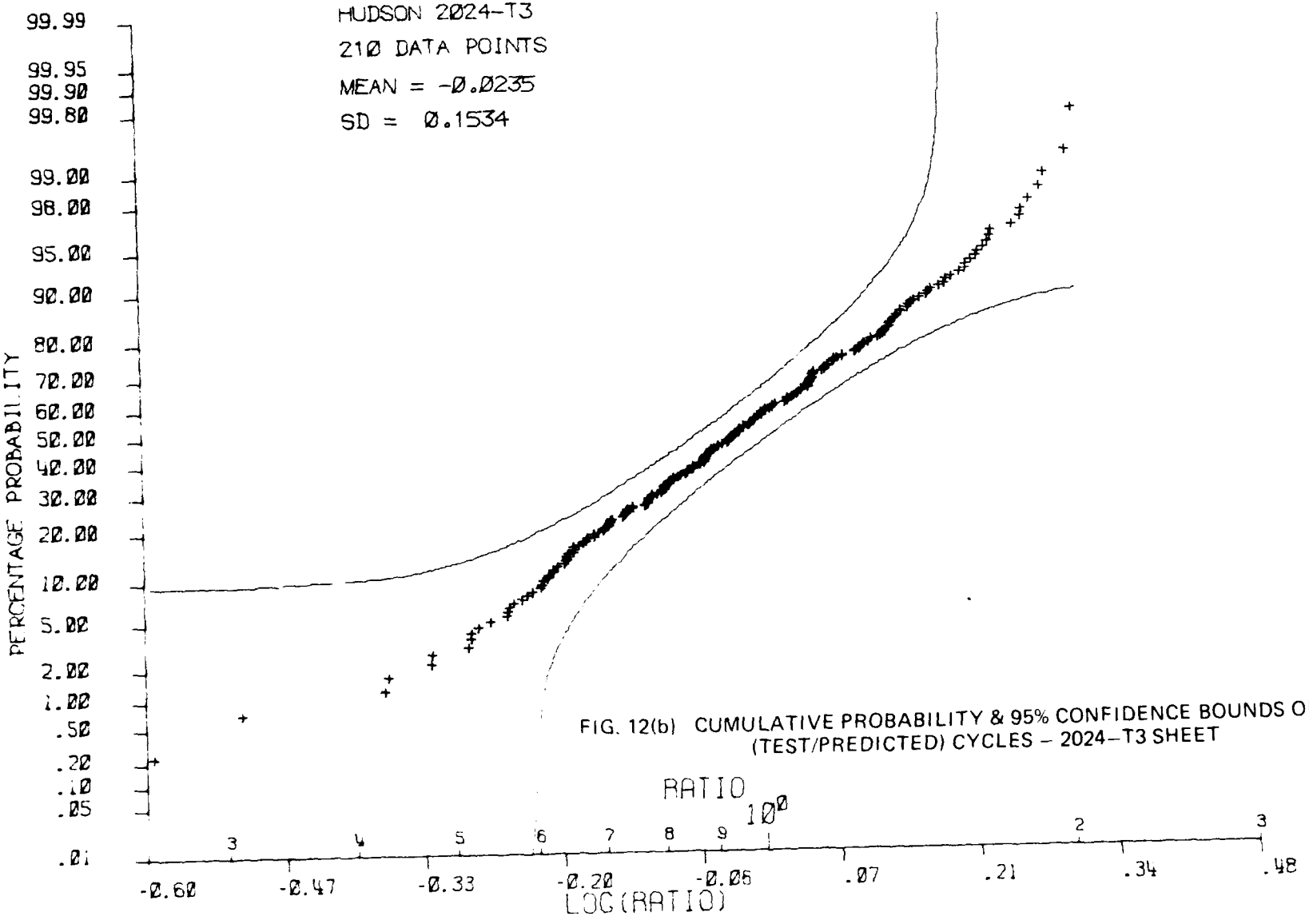

FIG. 12(b) CUMULATIVE PROBABILITY & 95% CONFIDENCE BOUNDS OF RATIO (TEST/PREDICTED) CYCLES – 2024–T3 SHEET

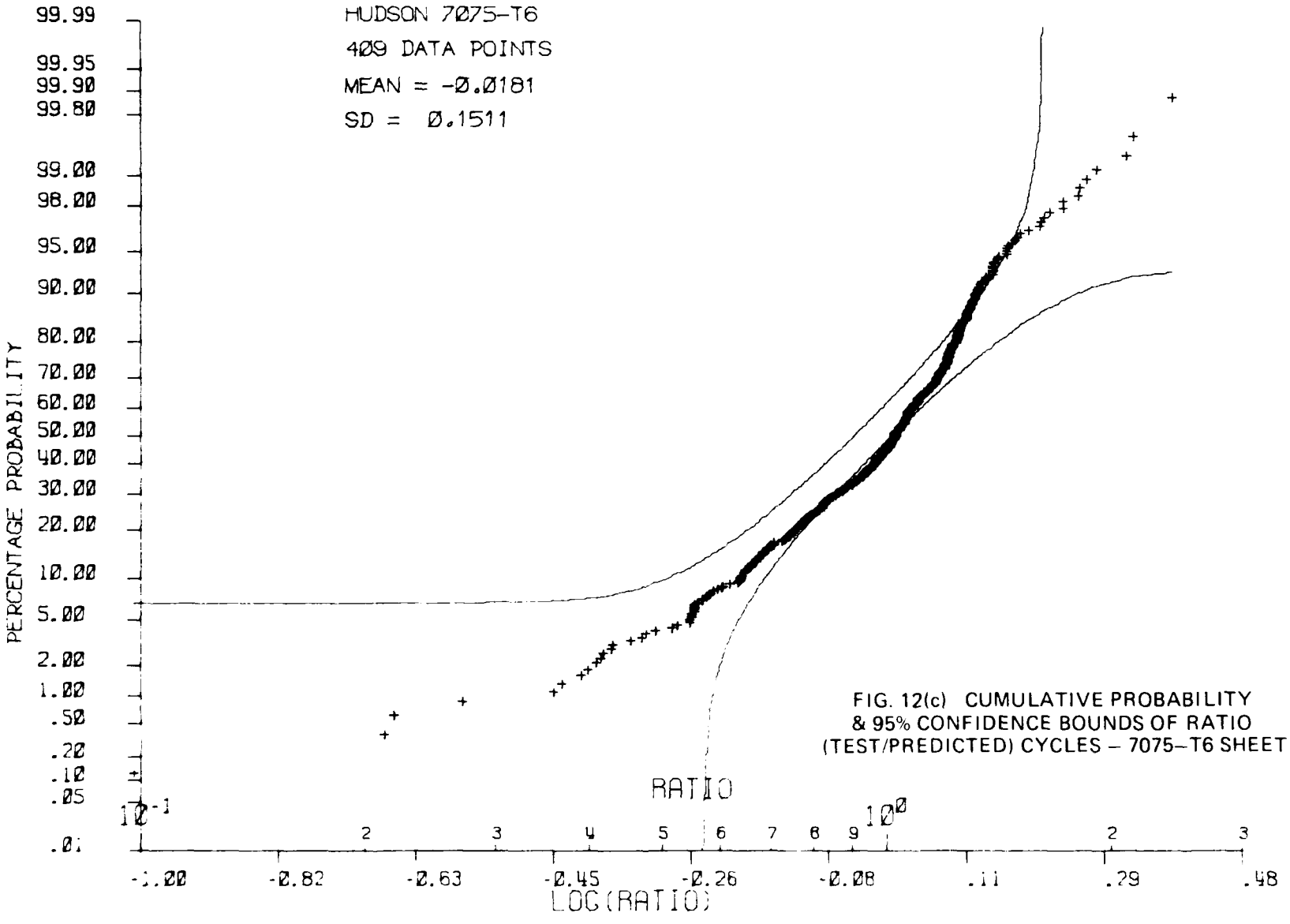

FIG. 12(c) CUMULATIVE PROBABILITY
& 95% CONFIDENCE BOUNDS OF RATIO
(TEST/PREDICTED) CYCLES – 7075–T6 SHEET

DISTRIBUTION

AUSTRALIA

Department of Defence

Central Office

Chief Defence Scientist	1
Deputy Chief Defence Scientist	2
Superintendent, Science and Technology Programmes	3
Aust. Defence Scientific and Technical Rep. (U.K.)	
Counsellor, Defence Science (U.S.A.)	
Defence Central Library	4
Document Exchange Centre, D.I.S.B.	5 21
Joint Intelligence Organisation	22

Aeronautical Research Laboratories

Chief Superintendent	23
Library	24
Superintendent Structures	25
Divisional File-Structures	26
Authors: G. S. Jost	27
L. R. Gratzer	28

Materials Research Laboratories

Library	29

Defence Research Centre

Library	30

Central Office

Director General Army Development (NSO) (4)	31 34

Central Studies Establishment

Information Centre	35

Engineering Development Establishment

Library	36

RAN Research Laboratory

Library	37

Victorian Regional Office

Library	38

Navy Office

Naval Scientific Adviser	39

Army Office

Army Scientific Adviser	40
Royal Military College Library	41

Air Force Office

Aircraft Research and Development Unit, Scientific Flight Group	42
Air Force Scientific Adviser	43
Technical Division Library	44

Department of Industry and Commerce

Government Aircraft Factories

Library	45


FILMED
4-8